



|                         |  |
|-------------------------|--|
| <b>Title</b>            | Magma dynamics and collapse mechanisms during four historic caldera-forming events   |
| <b>Author(s)</b>        | Stix, John; Kobayashi, Tomokazu  |
| <b>Citation</b>         | Journal of Geophysical Research. B, Solid earth, 113(9), B09205<br><a href="https://doi.org/10.1029/2007JB005073">https://doi.org/10.1029/2007JB005073</a> |
| <b>Issue Date</b>       | 2008-09-04   |
| <b>Doc URL</b>          | <a href="http://hdl.handle.net/2115/34998">http://hdl.handle.net/2115/34998</a>  |
| <b>Rights</b>           | An edited version of this paper was published by AGU. Copyright 2008 American Geophysical Union.   |
| <b>Type</b>             | article (author version)   |
| <b>File Information</b> | Stix_Kobayashi_JGR2008.pdf   |



[Instructions for use](#)

# Magma dynamics and collapse mechanisms during four historic caldera-forming events

*John Stix, Department of Earth and Planetary Sciences, McGill University, 3450  
University Street, Montreal, Quebec H3A 2A7, Canada*

*Tel +1-514-398-5391, Fax +1-514-398-4680, Email stix@eps.mcgill.ca*

*Tomokazu Kobayashi, Institute of Seismology and Volcanology, Graduate School  
of Science, Hokkaido University, Kita 10 Nishi 8, Kita-ku, Sapporo, 060-0810, Japan*

*Tel +81-11-706-3552, Email tkoba@uvo.sci.hokudai.ac.jp*

## **Abstract**

Four historic caldera-forming events were studied to understand the relationship of magma withdrawal processes and caldera subsidence mechanisms. Two calderas are silicic (Katmai 1912, Pinatubo 1991) and two are basaltic (Fernandina 1968, Miyakejima 2000). All events have sufficient geophysical, geologic, and petrologic data with which to examine and model magma withdrawal and caldera collapse. The data reveal that the magmas erupted at Katmai and Pinatubo were in a bubbly state in the reservoir immediately before and during caldera collapse. The bubbly magma allowed for its efficient extraction from the reservoir, causing significant underpressures to develop rapidly, particularly in the case of Katmai where the erupted rhyolite was voluminous, nearly aphyric, and very low viscosity. The rapidly developing underpressures at Katmai and Pinatubo caused sudden en masse caldera collapse halfway through the climactic eruptions, thereby liberating large amounts of seismic energy. At Fernandina and Miyakejima, by contrast, caldera collapse was initiated early and continued for an

30 extended period of time from weeks to months, consisting of a series of discrete  
31 subsidence events manifested by large earthquakes at Fernandina and by very long period  
32 (VLP) signals at Miyakejima. Systematic changes in earthquake magnitudes and  
33 quiescent intervals at both volcanoes reveal changes in friction as collapse took place  
34 during extended time intervals.

35

## 36 **1. Introduction**

37 Our understanding of calderas has increased significantly in recent years. This  
38 improvement is the result of new experimental and theoretical research which has  
39 complemented detailed field studies of calderas. By marrying these different approaches,  
40 we have gained important insight into the surface and subsurface workings of caldera  
41 systems. Experiments by *Roche et al.* [2000] have shown, for example, that the aspect  
42 ratio of the roof (thickness/width) plays an important role for the style of caldera  
43 collapse, with piston-style behavior at low aspect ratios and more piecemeal collapse at  
44 larger aspect ratios, often accompanied by subsurface stoping. *Roche and Druitt* [2001]  
45 developed a failure criterion for piston collapse which is related to the aspect ratio of the  
46 roof. Experiments by *Kennedy et al.* [2004] showed that many calderas are polygonal in  
47 nature rather than circular, due in part to crustal heterogeneities. Modelling by *Folch and*  
48 *Martí* [1998] and *Martí et al.* [2000] examined pressure variations during caldera-  
49 forming eruptions, while *Legros et al.* [2000] studied the effect of changing conduit  
50 geometry upon such large-scale eruptions. *Kumagai et al.* [2001] developed a pumping  
51 model of caldera subsidence, whereby changing pressures in the reservoir controlled the  
52 style and amount of subsidence.

53           Despite these impressive advances, there are a number of important unresolved  
54 questions regarding caldera formation. Perhaps most importantly, the timing of collapse  
55 is not well known for real calderas. Does subsidence begin at an early stage during the  
56 eruption, or does it commence at a later stage? Does subsidence occur in a continuous or  
57 incremental fashion throughout the eruption, or does it occur suddenly and en masse at  
58 some specific time? The aspect ratio of the roof may play an important role in the timing,  
59 with small values favoring early and/or incremental collapse, and large values resulting in  
60 late-stage en masse subsidence. The occurrence of lithic lag breccias interbedded with  
61 ignimbrite deposits can help shed light on the timing of collapse [e.g., *Druitt and Bacon*,  
62 1986]. Nevertheless, our understanding of this problem is still rudimentary. A second  
63 related issue is the relationship between magma withdrawal and caldera collapse. This  
64 question is important, since it bears upon the amount of underpressure, due to withdrawal  
65 of magma, which develops in the magma reservoir before the onset of subsidence. Third,  
66 the issue of collapse dynamics is still unresolved. Does subsidence occur as a response to  
67 magma withdrawal from the reservoir? Or does subsidence of the roof forcefully push  
68 magma out of the reservoir, in the process repressurizing the system [*Druitt and Sparks*,  
69 1984; *Martí et al.*, 2000; *Kumagai et al.*, 2001]? Finally, what is the effect of magma  
70 rheology upon the magma extraction and subsidence processes? For example, magmas  
71 that are poor in crystals may behave differently during their extraction compared to  
72 crystal-rich magmas. The extent to which a magma is compressible also may influence  
73 the amount of underpressure that develops due to magma withdrawal.

74           The purpose of this report is to explore these issues by examining four historic  
75 caldera-forming events which are well-documented and have adequate geologic and

76 geophysical data with which to address these questions. Of the four, two are silicic  
77 eruptions (Katmai 1912, Pinatubo 1991) and two are mafic (Fernandina 1968,  
78 Miyakejima 2000), thus providing both compositional similarities and contrast. For each  
79 example, the process of magma extraction is examined in relation to caldera collapse, as  
80 manifested by seismicity which was recorded at the time. Additionally, the magma  
81 rheology and dynamics are analyzed to study their effects upon underpressure generated  
82 by magma extraction, as well as upon the subsequent subsidence. The goal is to shed  
83 light on these and related issues by integrating observational, experimental, and  
84 theoretical data related to caldera formation.

85

## 86 **2. Chronology of Caldera Development**

### 87 **2.1. Katmai 1912**

88 Much of the following summary of the 1912 Katmai eruption draws upon the  
89 important papers by *Abe* [1992] and *Hildreth and Fierstein* [2000]. The climactic  
90 eruption of Katmai lasted 60 hours and erupted  $13.5 \text{ km}^3$  of magma (dense rock  
91 equivalent or DRE), frequently with simultaneous plinian and ignimbrite activity. The  
92 eruptive materials consisted of nearly aphyric rhyolite ( $7\text{-}8 \text{ km}^3$  DRE), dacite ( $4.5 \text{ km}^3$ ),  
93 and andesite ( $1 \text{ km}^3$ ), both with 30-50% crystals. The rhyolite was erupted at the  
94 beginning of the eruption and was predominant. The aspect ratio of the magma  
95 reservoir's roof was approximately 2, based on a thickness of 4-5 km and an average  
96 width of 2.3 km [*Hildreth and Fierstein*, 2000] (Table 1).

97 A critically important phase of the climactic eruption occurred at about 1000 UTC  
98 on 7 June (midnight local time on 6 June, the time difference being 10 hours), about 11

99 hours after the onset of the eruption. To this point, a cumulative amount of  $\sim 8.7 \text{ km}^3$   
100 DRE of magma had been erupted, representing 64% of the  $13.5 \text{ km}^3$  total volume, with  
101 an average evacuation rate of  $\sim 2.2 \times 10^5 \text{ m}^3 \text{ s}^{-1}$ . This  $8.7 \text{ km}^3$  volume was nearly all  
102 rhyolite; at this point in time, however, the relative proportions changed dramatically,  
103 with rhyolite decreasing to 40-50% and dacite and andesite increasing to  $\sim 40\%$  and  
104  $\sim 10\%$ , respectively. Subsequently, the evacuation rate declined abruptly to  $\sim 2.8 \times 10^4 \text{ m}^3$   
105  $\text{s}^{-1}$  well into 8 June. For a period of 5-6 hours on 7 June, the relative proportions of the  
106 three magma types fluctuated rapidly and substantially.

107 Seismicity during the climactic eruption was characterized by very high levels of  
108 liberated energy, mainly due to several large-magnitude earthquakes [Abe, 1992; Hildreth  
109 and Fierstein, 2000]. The pattern of seismicity exhibited several large, rapid jumps when  
110 plotted on a diagram of cumulative energy vs. time (Fig. 1a). Energies were calculated as  
111  $\log E = 1.96 M + 2.05$  where  $E$  is the energy in Joules and  $M$  the magnitude of the  
112 earthquake. The first significant increase occurred at 0956 UTC on 7 June, with a M 6.5  
113 earthquake coinciding with the change in magma compositions described above. This  
114 event may indicate the initiation of caldera collapse, since the first lithic mud layer was  
115 erupted from the volcano at this time, followed by a second mud layer approximately six  
116 hours later [Hildreth and Fierstein, 2000]. The second major jump began with a M 7.0  
117 earthquake at 0736 UTC on 8 June, followed by a M 6.8 event at 0848 UTC and a M 6.6  
118 event at 1300 UTC [Abe, 1992] (Fig. 1a). During this  $5\frac{1}{2}$  hour period, approximately  
119 60% of the total energy associated with the climactic eruption was released, likely  
120 corresponding with the bulk of caldera subsidence [Hildreth and Fierstein, 2000].

121 We have redrawn Figure 1 as a non-dimensional diagram (Fig. 2) where time is  
122 normalized to the duration of the climactic eruption, and cumulative energy is normalized  
123 to the total energy released during and immediately after the climactic eruption. At  
124 Katmai, there is a clear mismatch between erupted magma and released seismic energy  
125 during the climactic eruption, with significant amounts of magma being erupted well  
126 before the bulk of the seismic energy release (Fig. 2a). For example, by the first M 6.5  
127 earthquake at 0956 UTC on 7 June, ~64% of the total magma volume had already been  
128 erupted, while only ~4.5% of the cumulative seismic energy was released. At this stage,  
129 the eruption was less than 20% complete. By the time of the M 7.0 earthquake at 0736  
130 UTC on 8 June, approximately halfway through the climactic eruption, 80% of the  
131 magma had been erupted and 51% of the seismic energy released.

132 A final point is that of the total released seismic energy associated with caldera  
133 collapse at Katmai, 74% was released during the 60-hour climactic eruption. Thus, there  
134 was additional seismic energy released after the climactic eruption, which may be related  
135 to structural adjustments and further collapse of the unstable edifice.

136

## 137 **2.2 Pinatubo 1991**

138 The climactic phase of the 15 June 1991 Pinatubo eruption lasted approximately  
139 8.8 hours, beginning at 0542 UTC (1342 local time, the time difference being 8 hours)  
140 [Hoblitt *et al.*, 1996]. The eruptive products consisted almost entirely of dacite, with 3.7-  
141 5.3 km<sup>3</sup> of DRE magma erupted [Scott *et al.*, 1996]. According to these values, the mean  
142 magma discharge rate ranged from  $1.2 \times 10^5 \text{ m}^3 \text{ s}^{-1}$  to  $1.7 \times 10^5 \text{ m}^3 \text{ s}^{-1}$ . Koyaguchi and  
143 Ohno [2001] have suggested that initial discharge rates may have reached as high as 3.6 x

144  $10^5 \text{ m}^3 \text{ s}^{-1}$ , subsequently declining to  $\sim 1.2 \times 10^5 \text{ m}^3 \text{ s}^{-1}$  during the course of the eruption.  
145 The aspect ratio of the roof was  $\sim 2.4$ , based upon the observed caldera diameter of 2.5  
146 km and depth to the top of the magma reservoir of  $\sim 6$  km [Mori *et al.*, 1996a; Rutherford  
147 *and Devine*, 1996] (Table 1). This is a maximum value, as the lateral extent of the roof  
148 may have been greater at depth.

149 Significant seismicity began with a M 5.1 event at 0739 UTC on 15 June, two  
150 hours after the the beginning of the climactic eruption [Mori *et al.*, 1996b]. The pattern of  
151 cumulative seismic energy resembles that of Katmai, with large jumps occurring midway  
152 through the eruption (Fig. 1b). At 1041 UTC, a M 5.5 event was recorded, and 34  
153 minutes later at 1115 UTC, the largest earthquake of the sequence (M 5.7) was observed.  
154 The bulk of caldera collapse may have occurred at the time of these large-magnitude  
155 events [Scott *et al.*, 1996], although there is some uncertainty as to whether the  
156 earthquakes were related directly to collapse or were tectonic in origin [Bautista *et al.*,  
157 1996]. Lithic breccias and lithic-rich pyroclastic flow deposits were observed to overlie  
158 most of the pumiceous pyroclastic flow deposits [Scott *et al.*, 1996], also suggesting that  
159 the majority of collapse took place at a relatively late stage during the climactic eruption.

160 Similar to Katmai, there is a mismatch in timing between erupted magma and  
161 released seismic energy (Fig. 2b). By the time of the M 5.5 earthquake at 1041 UTC, at  
162 least 57% of the total magma volume of  $3.7\text{-}5.3 \text{ km}^3$  had been erupted, while only 14% of  
163 cumulative energy was released. The value of 57% may in fact be appreciably larger if  
164 discharge rates were high during early stages of the climactic eruption, as suggested by  
165 *Koyaguchi and Ohno* [2001]. When the M 5.7 event occurred at 1115 UTC, at least 63%



166 of the magma had been erupted, with 43% of the cumulative energy released. At this  
167 stage, the climactic eruption was nearly two thirds complete.

168         Compared to Katmai, proportionally more seismic energy was released at  
169 Pinatubo after the climactic eruption stopped (51% for Pinatubo vs. 26% for Katmai) than  
170 during the eruption itself. Discharge rates at Pinatubo appear to be higher than at Katmai,  
171 while the climactic eruption was significantly shorter. As a result, structural adjustments  
172 after the climactic eruption may have been more significant at Pinatubo than at Katmai.

173

### 174 **2.3 Fernandina 1968**

175         By contrast with Katmai and Pinatubo, caldera development at Fernandina in  
176 1968 occurred over an extended period of 250-300 hours between 12-21 June [*Simkin*  
177 *and Howard, 1970; Filson et al., 1973*]. The magma was basaltic in composition. Nearly  
178 all magma displacement occurred beneath the surface, with only a small amount erupted.  
179 A caldera was already present when this collapse episode took place. During 12-21 June  
180 1968, the caldera floor subsided a maximum of 350 m in the southeast sector. A pre-  
181 existing tuff cone on the caldera floor was observed to be undisturbed after the collapse  
182 event [*Simkin and Howard, 1970; Filson et al., 1973*]. These observations suggest  
183 trapdoor-style piston subsidence. The new collapse volume at the surface was 2.0-2.4  
184 km<sup>3</sup>. Based upon a 1 km-thick roof and a 3200 m equivalent diameter of the caldera floor,  
185 the aspect ratio of the roof was ~0.3 (Table 1), although there is some uncertainty of the  
186 roof thickness [*Filson et al., 1973*].

187         The sequence of events began with an eruption accompanied by lava flows which  
188 were observed on the eastern flank of the volcano on 21 May 1968. A possible explosion

189 occurred on 8 June at 0220 UTC (2020 local time on 7 June, the time difference being 6  
190 hours). On 11 June, a vapor cloud was observed after a M 3 earthquake at 1618 UTC.  
191 This emission was followed by two large explosive eruptions at 2218 and 2308 UTC  
192 which may have been partly phreatomagmatic [*Simkin and Howard, 1970; Filson et al.,*  
193 *1973*]. After these events, significant amounts of lithic-rich tephra began to fall, an  
194 occurrence which may have marked the initiation of caldera collapse [*Simkin and*  
195 *Howard, 1970*]. Eruptive activity then diminished on 12 June, while seismic activity  
196 increased, with a series of  $M \geq 5$  earthquakes beginning at 2221 UTC [*Filson et al.,*  
197 *1973*]. These large earthquakes probably represented the early stages of caldera  
198 subsidence. Mean minimum magma evacuation rates were  $3.0\text{-}3.4 \times 10^3 \text{ m}^3 \text{ s}^{-1}$ , based on  
199 a caldera collapse volume of  $2.2 \times 10^9 \text{ m}^3$  and a duration of 182 hours from 12-20 June  
200 for subsurface drainage of magma from the reservoir. These rates are several orders of  
201 magnitude less than at Katmai and Pinatubo.

202         The seismicity associated with collapse at Fernandina was exceptional [*Filson et*  
203 *al., 1973*]. From 2221 UTC on 12 June to 0420 UTC on 15 June, there were a series of M  
204  $\geq 5$  events which were regularly spaced at  $\sim 6$  hours. Beginning at 0851 UTC on 15 June,  
205 the large events decreased (a) in magnitude to M 4.7-4.9 and (b) in spacing to  $\sim 4$ -hour  
206 intervals. Starting late on 16 June or early on 17 June, the seismic pattern changed yet  
207 again, with more closely spaced events of generally smaller magnitudes (i.e., M 4.0-4.5).  
208 At about 1200 UTC on 20 June, the number of earthquakes decreased rapidly. For  
209 example, 89 events were recorded on 20 June, 13 on 23 June, and only 5 on 24 June  
210 [*Filson et al., 1973*]. Recorded seismicity stopped on 27 July.

211 By contrast with Katmai and Pinatubo, the overall pattern of seismic energy  
212 released by Fernandina during caldera subsidence was quite regular, showing initially  
213 high rates of energy which gradually subsided with time to zero (Fig. 1c). The trend  
214 between 25-75 hours is characterized by a series of abrupt jumps, which are the M 5  
215 events occurring mainly on 13-14 June. The jumps then become smaller and eventually  
216 indiscernible on the diagram by 150 hours as earthquakes diminished in magnitude and  
217 increased in number.

218

#### 219 **2.4 Miyakejima 2000**

220 Caldera development at Miyakejima from 8 July of 2000 was even more  
221 protracted than at Fernandina, extending over a period of about 40 days. However, the  
222 nature of magma evacuation at Miyakejima resembled that at Fernandina. The total  
223 volume of the caldera of  $6 \times 10^8 \text{ m}^3$  [Geshi *et al.*, 2002] is much larger than the volume of  
224 ejecta from the eruption ( $9.3 \times 10^6 \text{ m}^3$ ) [Nakada *et al.*, 2005], since magma was  
225 displaced almost entirely in the subsurface, with very little material being erupted. The  
226 caldera was intermittently enlarged during July-August 2000, and its final size was 1.6  
227 km in diameter and 450 m in depth [Geshi *et al.*, 2002]. The depth of the magma  
228 chamber related to caldera formation is not well-known, but seismic and geodetic surveys  
229 suggest that a pressure source is located at a depth of 3-6 km [Kobayashi *et al.*, 2003;  
230 Irwan *et al.*, 2003; Ueda *et al.*, 2005]. Using 3-6 km as the thickness of the caldera block,  
231 the aspect ratio of the roof is evaluated as  $1.9 \sim 3.8$ .

232 The magmatic activity began with a gigantic seismic swarm on 26 June around  
233 0859 UTC (1759 local time on 26 June, the time difference being 9 hours) [Ueda *et al.*,

234 2005; *Uhira et al.*, 2005] caused by northwestward dike-forming intrusions of magma,  
235 followed by a small submarine eruption [*Nakada et al.*, 2005; *Kaneko et al.*, 2005]. The  
236 earthquake swarm beneath the island died out by the next day, and activity shifted to a  
237 comparatively quiescent stage. However, small volcanic earthquakes began to be  
238 recorded beneath the summit at the beginning of July, leading to a summit eruption on 8  
239 July at 0941 UTC, accompanied by significant subsidence at the surface. A void was  
240 already present just beneath the summit several days before the first summit eruption, so  
241 that the subsidence on 8 July is interpreted as collapse of a block into a shallow void  
242 space [*Furuya et al.*, 2003]. The caldera grew incrementally after the eruption [*Geshi et*  
243 *al.*, 2002], with infrequent explosive eruptions. The caldera had grown to about 1.5 km in  
244 diameter by early August and was widened later by landslides off its steep walls [*Nakada*  
245 *et al.*, 2005]. Intermittent explosive eruptions that had occurred from 10 August  
246 eventually led to the largest explosion on 18 August around 0900 UTC which was  
247 vulcanian to subplinian in nature. After this eruption, significant caldera development  
248 was not observed. The caldera size finally reached  $\sim 0.6 \text{ km}^3$  in volume [*Geshi et al.*,  
249 2000]. Based on the duration between the first summit subsidence on 8 July and the  
250 largest eruption on 18 August (984 hours), the mean magma evacuation rate is estimated  
251 at  $\sim 170 \text{ m}^3 \text{ s}^{-1}$ . The rate is significantly less than the other three volcanoes. After the  
252 largest eruption, the characteristic activity was strong degassing. By the end of August  
253 and early September, the volcano began to emit substantial quantities of sulfur dioxide, at  
254 times exceeding 100,000 metric tonnes  $\text{SO}_2$  per day [*Kazahaya et al.*, 2004].

255         The seismic activity during caldera formation was characterized by very long-  
256 period (VLP) seismic pulses having a pulse width of about 50 seconds [*Kikuchi et al.*,

257 2001; Kumagai *et al.*, 2001]. A series of VLP signals were observed once or twice a day  
258 from 9 July at 1339 UTC to 17 August at 1907 UTC. This period corresponds exactly  
259 with the observed duration of caldera development. The equivalent moment magnitudes  
260 are 5.0 to 5.6, according to Kikuchi *et al.* [2001]. In addition to the VLP signals, other  
261 earthquakes occurred during the caldera formation stage, e.g., series of earthquakes  
262 which were observed as precursors to the VLP signal [Kobayashi *et al.*, 2003], but the  
263 magnitude of these individual events was only 1 to 2. Thus, the total released seismic  
264 energy during caldera development can be generally described by the VLP signals alone  
265 (Fig. 3). The released seismic energy of each VLP event is calculated as  $\log E_s = \log M_0 -$   
266  $4.3$ , where the seismic energy  $E_s$  is in Joules and the seismic moment  $M_0$  is in Nm. The  
267 overall trend of released seismic energy is similar to that of Fernandina; the seismic  
268 energy was regularly released at a nearly constant rate, unlike the pattern of Katmai and  
269 Pinatubo. In early stages, the occurrence interval was approximately 12 h, but it became  
270 substantially longer at the beginning of August ( $\sim 500$  h on Fig. 3), with magnitudes of  
271 individual VLP events correspondingly increasing. This trend of occurrence is opposite to  
272 the case of Fernandina. The repetitious character of these VLP signals, as well as the  
273 constant growth rate of the caldera, implies that the subsidence process at Miyakejima  
274 was highly regular and systematic. Kumagai *et al.* [2001] have interpreted these signals  
275 as a volumetric expansion of the magma reservoir which may be associated with slip of a  
276 vertical piston in the conduit, followed by magma outflow and gradual depressurization.  
277 Slow deflation was recorded by the tiltmeters on the island [e.g., Ukawa *et al.*, 2000]  
278 during the interval of VLP occurrence representing rapid short-term inflations of the  
279 magma reservoir. Thus, these seismic events can describe a basic framework of magma

280 withdrawal on short timescales controlling caldera development, a process which is  
281 superimposed upon deformation trends at longer timescales. This may be a common  
282 feature for other volcanoes as well.

### 283 **3. Modelling the Subsidence Process**

284 The high aspect ratios of the Katmai and Pinatubo caldera blocks illustrate the  
285 presence of comparatively thick crust which likely provided “bridging” roof support for  
286 the magma reservoirs beneath. Accordingly, Katmai and Pinatubo illustrate the mismatch  
287 between early magma withdrawal and comparatively late caldera collapse. By contrast,  
288 magma withdrawal and caldera subsidence at Fernandina and Miyakejima appear to have  
289 taken place during short intervals and in a progressive manner. In the case of Fernandina,  
290 the thin roof may not have provided much support or resistance before or during  
291 subsidence. Miyakejima is a more complicated case which exhibited both a thin roof  
292 during initial caldera collapse [*Kikuchi et al.*, 2001], as well as a thicker crustal block  
293 which subsided in a progressive fashion during the summer of 2000. These differences  
294 pose interesting questions regarding the properties of the magmas, the nature of the  
295 magma withdrawal process, and the dynamics of caldera formation during these  
296 eruptions.

297 Because the eruptions have been well studied, many parameters relating to the  
298 eruptions are well constrained, and the eruptions thus can be modeled with some  
299 confidence in terms of magma withdrawal and caldera development. *Kumagai et al.*  
300 [2001] have modeled caldera subsidence at Miyakejima in the middle of 2000. Their  
301 approach can be adapted for use at Katmai, Pinatubo, and Fernandina with certain  
302 caveats, in particular that caldera subsidence occurs as a piston-style process. By this, we

303 mean that the roof of the magma reservoir subsided coherently as a single block. This  
 304 style of subsidence is illustrated schematically in Figure 4. We recognize that many  
 305 calderas have more complicated subsidence styles, such as piecemeal, downsagging, a  
 306 series of concentric downthrown blocks, etc. [Kennedy and Stix, 2003]. Nevertheless,  
 307 while this collapse style is likely an oversimplification, it is sufficient for the modelling  
 308 presented here, since Katmai and Pinatubo collapsed en masse and Fernandina and  
 309 Miyakejima as a series of discrete steps. Kumagai *et al.* [2001] show that the piston  
 310 begins to move downward after a time  $T$ :

311

$$312 \quad T = \frac{2(F_s - F_d)}{313 \quad p'A} \quad (1)$$

314

315  
 316 where  $F_s - F_d$  are static and dynamic frictions, respectively,  $p'$  is the rate of pressure  
 317 decrease due to outflow of magma from the magma chamber, and  $A$  is the cross-sectional  
 318 area at the base of the piston (all symbols are explained in Table 2). Equation (1) can be  
 319 rewritten as

320

$$321 \quad p'TA > 2(F_s - F_d) \quad (2)$$

322

323 which shows that the piston will move downward when the pressure decrease  $p'T$   
 324 exceeds the rock friction or rock strength. Kumagai *et al.*'s [2001] model is essentially  
 325 one of repeatedly pumping the magma chamber with the piston:

326

$$327 \quad p_1 = p_0 - p'T + p \quad (3)$$

328

329 where  $p_0$  is the original pressure in the magma chamber,  $p'T$  is the pressure decrease due330 to magma outflow,  $p$  is the pressure increase in the chamber once the caldera block331 begins to move downward, and  $p_1$  is the re-equilibrated pressure in the magma chamber.

332 The equation describes a stick-slip sense of movement of the caldera block, where stick is

333 associated with underpressure as magma is erupted or drained from the reservoir. After a

334 certain time, underpressure exceeds friction, and the block begins to slip. This movement

335 may squeeze the magma, causing it to be repressured. Equation (3) can be written as

336

337 
$$p_1 = p_0 + \kappa[(-\alpha T + Az) / V_0] \quad (4)$$

338

339 where  $\kappa$  is the bulk modulus of the magma,  $\alpha$  the evacuation rate of the magma,  $z$  the340 displacement of the block, and  $V_0$  the initial volume of the magma chamber before341 caldera subsidence is initiated [*Kumagai et al.*, 2001].

342 With respect to events at Katmai and Pinatubo, we are interested primarily in

343 pressure variations of the magma reservoir before the bulk of collapse occurred. As

344 observed in Figures 1-2 above, there was an extended period of magma withdrawal

345 before the bulk of collapse was initiated approximately halfway through the climactic

346 eruptions, as manifested by the sudden onset of large-scale seismicity. This period of

347 magma withdrawal indicates that pressure was decreasing in the magma reservoirs at

348 both volcanoes. The pressure decrease prior to caldera subsidence can be calculated as

349 follows:

350



351  
352  
353  
354

$$p'T = \frac{\kappa\alpha T}{V_0} \quad (5)$$

355 For Katmai and Pinatubo, we assume that the bulk of collapse occurred in a short  
356 time interval about halfway through the climactic eruption. For Fernandina, collapse  
357 occurred incrementally separated by quiescent intervals of six hours. The parameters  $T$ ,  $\alpha$ ,  
358 and  $V_0$  are reasonably constrained at all three volcanoes (Table 1), while  $\kappa$  is not.  
359 Therefore, we have plotted the pressure decrease against a range of bulk moduli in Figure  
360 5. For Katmai and Pinatubo, bulk moduli range from  $\sim 10^6$  Pa to  $10^{10}$  Pa for pressure  
361 decreases from 1 MPa to nearly 10 GPa, respectively.

362 Equations (2) and (5) are valid once the caldera collapse process is in a steady-  
363 state condition, i.e., the caldera block is alternately sticking and slipping during the  
364 course of subsidence. At Katmai and Pinatubo, however, this condition may not be  
365 strictly true, as the evacuating magma reservoir and increasing underpressure were  
366 developing before the bulk of subsidence was initiated. Here, the resistance to subsidence  
367 was provided by the shear strength and fracture processes of the country rocks. In this  
368 case, an independent approach for estimating underpressures is to use the failure criterion  
369 method of *Roche and Druitt* [2001], which calculates the underpressure  $p'T_{\text{crit}}$  which is  
370 required to exceed a critical shear stress upon the rocks above the magma reservoir:

371  
372  
373

$$p'T_{\text{crit}} \geq 4R\tau_c \quad (6)$$

374 where  $R$  is the aspect ratio of the caldera block as defined by its thickness  $H$  divided by  
 375 its diameter  $D$ , and  $\tau_c$  is the critical shear stress for failure. This shear stress can be solved  
 376 as follows:

377

$$378 \quad \tau_c = \tau_o + \mu\sigma_n \quad (7)$$

379

380 where  $\tau_o$  is the cohesion of the caldera block,  $\mu$  is the coefficient of internal friction of the  
 381 block ( $\sim 0.6$ ) [Byerlee, 1978], and  $\sigma_n$  is the mean stress normal to the plane of failure. This  
 382 last parameter can be calculated as  $\sigma_n = kp_{\text{lith}}$  where  $k$  is a constant ( $\sim 0.6$ ) [Cornet and  
 383 Valette, 1984],  $p_{\text{lith}}$  is the lithostatic pressure  $\rho_r g H/2$ ,  $\rho_r$  is the average density of the  
 384 caldera block, and  $g$  is the acceleration due to gravity.

385 Using these equations gives underpressures of 166-205 MPa for Katmai and 265-  
 386 312 MPa for Pinatubo for a range of cohesions from 0.1 MPa to 5 MPa [Roche and  
 387 Druitt, 2001]. These values may be overestimates, as shear strengths of rocks beneath  
 388 volcanoes are typically on the order of 1-100 MPa [Martí et al., 2000]. Nevertheless,  
 389 these calculations provide a useful upper limit of underpressures at these two volcanoes,  
 390 while our calculations from Equation (5) use a lower limit of 1 MPa. For these levels of  
 391 underpressure, therefore, bulk moduli for Katmai range from a low of  $1.2 \times 10^6$  Pa to a  
 392 high of  $2.0\text{-}2.5 \times 10^8$  Pa, while for Pinatubo the range is from  $2.0 \times 10^6$  Pa to  $5.2\text{-}6.1 \times$   
 393  $10^8$  Pa (Fig. 5). The bulk modulus for bubble-free magma is  $\sim 10^{10}$  Pa, while that for  
 394 bubbly magma is typically  $10^7\text{-}10^9$  Pa [Huppert and Woods, 2002]. It is thus reasonable  
 395 to conclude that reservoir magmas at Katmai and Pinatubo were bubbly immediately  
 396 before and during caldera collapse.

397 For Fernandina, the case is less clear, as pressure decreases range from ~0.3 MPa  
398 to ~290 MPa for bulk moduli of  $10^7$ - $10^{10}$  Pa (Fig. 5). This large range can be further  
399 constrained by the approach of *Roche and Druitt* [2001], as done above for Katmai and  
400 Pinatubo, and these calculations result in maximum critical underpressures of 3-9 MPa  
401 for Fernandina using the same range of cohesions as above. The comparatively low  
402 magma evacuation rates at Fernandina ( $10^3$  m<sup>3</sup> s<sup>-1</sup> compared to  $10^4$ - $10^5$  m<sup>3</sup> s<sup>-1</sup> at Katmai  
403 and Pinatubo) also imply relatively small amounts of underpressure. Thus, we suggest  
404 that the basaltic magma in the reservoir beneath Fernandina also had a reduced bulk  
405 modulus and appreciable vesicularity as it drained in the subsurface (Fig. 5).

406 It is important to assess the quality of the values we have used in these  
407 underpressure calculations, in particular the parameters  $T$ ,  $\alpha$ , and  $V_0$  (Table 1). In the case  
408 of  $T$ , we are fairly confident of the data, since they are constrained (1) by the time  
409 between the start of the climactic eruption and the sudden onset of large-scale seismicity  
410 for Katmai and Pinatubo, or (2) by the periods of seismic quiet between major  
411 earthquakes at Fernandina. For  $\alpha$ , the values we have used for Katmai and Pinatubo  
412 appear reasonable, as they are constrained by the volume of magma erupted during the  
413 course of the climactic eruption divided by its duration. Further refinements based on  
414 field studies have been possible for both volcanoes [*Hildreth and Fierstein*, 2000;  
415 *Koyaguchi and Ohno*, 2001]. For Fernandina, the case is not so clear because very little  
416 magma was erupted. Thus, we have used the caldera collapse volume at the surface  
417 divided by the duration of the collapse events. This is probably a minimum rate, so we  
418 have doubled this value to provide an upper limit. Lastly, the  $V_0$  parameter is not  
419 particularly well constrained. Thus we have simply used the volumes of erupted magma

420 (Katmai, Pinatubo) or caldera collapse volume (Fernandina) to represent  $V_0$ . These are  
 421 clearly minimum values; however, larger values of  $V_0$  would result in decreased  
 422 underpressures and bulk moduli (Fig. 5), reinforcing the argument that the magmas were  
 423 bubbly upon evacuation. A magma reservoir which empties itself entirely during a  
 424 climactic eruption is an interesting concept [*Martí et al.*, 2000]. Such conditions might  
 425 promote its replenishment during and/or immediately after the eruption [e.g., *Stix and*  
 426 *Gorton*, 1993]. Another possibility is a larger magma reservoir in which the largely liquid  
 427 portion is erupted while the more crystallized portion is not.

428 In these calculations, the  $T$  parameter is of crucial importance, since it is directly  
 429 related to the amount of underpressure that is generated before the roof fails and the bulk  
 430 of caldera collapse is initiated. It is thus essential to know if the  $T$  parameter is being used  
 431 appropriately and correctly in the calculations above. This can be verified by calculating  
 432 the displacement of the subsiding caldera block as follows. If  $T$  is significantly longer  
 433 than the duration of piston displacement, as appears to be the case for Katmai and  
 434 Pinatubo and probably Fernandina as well (Figs. 1, 2), then the displacement of the  
 435 caldera block can be estimated thus:

436

$$437 \quad z = \alpha T / A \quad (8)$$

438

439 Results for Katmai and Pinatubo are shown in Figure 6 and Table 3. Since magma  
 440 evacuation rates likely varied during the course of the climactic eruptions, we have used a  
 441 range of values from the minimum and maximum estimates. Allowing for some

442 uncertainty in the magma evacuation rates, the agreement between calculated and  
443 observed displacements is good (Table 3).

444 Equation (8) also can be used to examine the nature of subsidence at Fernandina.  
445 In this case,  $T$  and  $A$  are known while  $\alpha$  is not. Figure 7 shows the effects of evacuation  
446 rate and time before subsidence on the amount of displacement of the piston. For  
447 evacuation rates ranging from a minimum of  $2970 \text{ m}^3 \text{ s}^{-1}$  to a maximum of  $6730 \text{ m}^3 \text{ s}^{-1}$ ,  
448 individual displacements are 8-18 m, respectively. Notably, the spacing between major  
449 earthquakes changed on 15 June from 6 hours to 4 hours, with a corresponding decrease  
450 in the magnitudes of the earthquakes. Inputting these intervals as values for  $T$  reveals that  
451 individual displacements, as manifested by the earthquakes, decreased on 15 June from  
452 8.0 m to 5.4 m, using a constant evacuation rate of  $2970 \text{ m}^3 \text{ s}^{-1}$ . In summary, it is certain  
453 that (a) subsidence at Fernandina was incremental, in contrast to Katmai and Pinatubo,  
454 and (b) the amount of displacement for individual subsidence events declined with time.  
455 It is possible that both declining evacuation rates and time intervals between earthquakes  
456 contributed to these decreasing displacements. Alternatively, the evacuation rate  
457 remained approximately constant, and the smaller displacements were the result of  
458 reduced time intervals between earthquakes. This issue is examined more fully in the next  
459 section.

460

#### 461 **4. Discussion**

462 The analysis above has relevance for the dynamics of magma extraction, the  
463 nature of caldera subsidence, the presence of bubbly magma stored in shallow magma

464 reservoirs, and the progressive weakening of caldera faults. Furthermore, it is clear that in  
465 many cases these issues are inter-related. These points are discussed in turn below.

466

#### 467 **4.1 Early Extraction and Eruption of Silicic Magma at Katmai and Pinatubo**

468 The bulk of caldera collapse appears to have occurred midway through the  
469 climactic eruptions at Katmai and Pinatubo. Most of the magma was withdrawn and  
470 erupted rapidly in the early stages of the eruptions, allowing significant underpressures to  
471 quickly develop in the magma reservoirs. The early-erupted magma was highly  
472 extractable, principally due to its low viscosity. In the case of rhyolite magma at Katmai,  
473 for example, viscosity calculations using the method of *Hess and Dingwell* [1996]  
474 indicate that viscosities ranged from a maximum of  $1.4 \times 10^5$  Pa s at 4 wt. % H<sub>2</sub>O and  
475 805° C to a minimum of  $7.1 \times 10^3$  Pa s at 7 wt. % H<sub>2</sub>O and 850° C [*Westrich et al.*, 1991;  
476 *Lowenstern*, 1993; *Cowee et al.*, 1999; *Hildreth and Fierstein*, 2000; *Coombs and*  
477 *Gardner*, 2001]. As magma transited the conduit, flow was likely shearing at high strain  
478 rates. Under these conditions, viscosities would be lowered even further due to shear  
479 thinning behavior induced by the presence of bubbles [*Stein and Spera*, 2002] and/or  
480 viscous dissipation effects [*Lavallée et al.*, 2007]. It is therefore possible that the  
481 viscosity of rhyolite magma at Katmai approached values as low as  $10^3$  Pa s, which is  
482 similar to the viscosity of dry basalt [*Khitarov et al.*, 1976]. These low viscosities thus  
483 allowed rapid extraction of the early-erupted magma from the reservoir, causing high  
484 underpressures to develop as shown by Equation (5). High magma extraction rates also  
485 may have been aided by large pressure gradients due to the free gas phase and by large  
486 conduit dimensions.

487 Equation (5) also reveals that there may be a delicate balance between the bulk  
488 modulus and evacuation rate of the magma as a system is underpressured. In order to  
489 maintain reasonable underpressures ( $\sim 100$  MPa), bubbly magmas of low bulk modulus  
490 may be associated with high magma evacuation rates while bubble-poor magmas of high  
491 bulk modulus may be extracted at lower evacuation rates [*Huppert and Woods, 2002*].

492 At Katmai, a rheological interface was reached in the magma chamber at an early  
493 stage in the eruption when significant amounts of mixed crystal-rich dacite and andesite  
494 began to be erupted at  $\sim 1000$  UTC on 7 June. Significant seismicity was initiated at this  
495 point, while the volumetric eruption rate decreased by nearly an order of magnitude.  
496 These changes likely are the result of the eruption's tapping a rheological boundary  
497 between low-viscosity rhyolite above and high-viscosity dacite and andesite underneath.  
498 Using the underpressure arguments from above, the bulk modulus also may have changed  
499 abruptly at this boundary from low values in rhyolite to high values in dacite and  
500 andesite. The seismicity may indicate onset of caldera collapse; if so, subsidence of the  
501 caldera block may have helped mix dacite and andesite.

502 Rheological boundaries in silicic magma chambers may be common occurrences,  
503 serving to slow or stop the course of an eruption [*Smith, 1979, Bacon and Druitt, 1988;*  
504 *Scaillet et al., 1998; Hildreth, 2004*]. At the 121 Ma Ossipee ring complex in New  
505 Hampshire, *Kennedy and Stix [2007]* have shown that crystal-poor rhyolite was erupted,  
506 resulting in caldera subsidence. After collapse, crystal-rich quartz syenites were intruded  
507 into the ring dyke. The magma chamber configuration thus consisted of low-viscosity  
508 rhyolite magma which was erupted from the top of the reservoir, underlain by high-  
509 viscosity quartz syenite crystal mush which was not extractable and not erupted.

510 In summary, magma rheology and rheological boundaries appear to strongly  
511 influence the course of caldera-forming eruptions. For such systems, the nature of magma  
512 extraction has profound implications for the timing and nature of caldera subsidence.

513

#### 514 **4.2 Magma Extraction, Caldera Subsidence, and Seismic Energy Release**

515 *Hildreth and Fierstein* [2000] have shown that the seismic energy released at  
516 Katmai was 2-3 orders of magnitude higher than that observed at Pinatubo and  
517 Fernandina (and Miyakejima as well), attributing this difference to high-strength rocks,  
518 lateral magma flow, and horizontally layered structure at Katmai. As noted above, a  
519 comparatively large volume of magma was withdrawn and erupted at Katmai prior to the  
520 bulk of collapse. Experiments by *Roche et al.* [2000] and *Kennedy et al.* [2004] have  
521 shown that high aspect ratios of the caldera block result in late collapse after a significant  
522 volume of magma has been extracted from the reservoir. Such a situation allows large  
523 underpressures to develop in the reservoir before collapse is initiated. The experiments  
524 also reveal that subsidence occurs in a progressive fashion by stopping at low evacuation  
525 rates. In the case of high evacuation rates, however, we theorize that collapse may occur  
526 en masse after a significant proportion of magma has been withdrawn quickly from the  
527 reservoir, the subsidence involving a large fault surface area and significant slip. This  
528 style of collapse could be further facilitated by explosive enlargement of the ring fault or  
529 faults. In such a situation, the high seismic moment is principally the result of a large  
530 quantity of easily extractable magma which is erupted at a high rate from a deep  
531 reservoir, thus generating significant underpressure in a short period of time. The  
532 elevated evacuation rates result in a focusing of stress [*Sunde et al.*, 2004], causing the



533 crust to fail catastrophically along major caldera faults. The ensuing caldera collapse  
534 occurs abruptly, releasing large amounts of seismic energy. If this hypothesis is correct, it  
535 implies that this style of collapse is closely linked to the depth of the magma reservoir,  
536 the magma's rheology, and the extraction rate of the magma.

537

### 538 **4.3 Bubbly Magma in Shallow Reservoirs**

539 The bulk modulus of a substance is a measure of its incompressibility. It is a  
540 balance between an imposed pressure difference and the associated volume change of the  
541 material:

542

$$543 \quad \kappa = \frac{\Delta p}{\Delta V / V_0} \quad (9)$$

544  
545  
546

547 Where  $\Delta p$  is the pressure difference and  $\Delta V$  the change in volume. The calculations  
548 above demonstrate that the Katmai and Pinatubo reservoir magmas were in a bubbly state  
549 during their extraction prior to the bulk of caldera collapse. However, the calculations do  
550 not reveal the physical state of the magmas before the initiation of magma withdrawal.

551 They may have been undersaturated, saturated, or oversaturated in volatiles. Other lines  
552 of evidence indicate that a pre-eruptive, separate fluid phase was present beneath  
553 Pinatubo [Wallace and Gerlach, 1994] and possibly Katmai [Coombs and Gardner,  
554 2001; Hammer *et al.*, 2002]. It is thus reasonable to infer that these magmas may have  
555 been partly vesicular before eruption, thereby aiding their extraction from the reservoir.

556 The occurrence of bubble-rich magma in shallow reservoirs has important  
557 ramifications for eruptive processes. Such magma will have high buoyancy and low

558 viscosity, particularly so if the magma contains few crystals; as a result, it will be mobile  
559 and easily extracted and erupted from the reservoir. These properties can explain the high  
560 eruption rates observed during the early stages of the Katmai and Pinatubo eruptions  
561 [*Hildreth and Fierstein, 2000; Koyaguchi and Ohno, 2001*] and are consistent with  
562 *Huppert and Woods'* [2002] model which shows enhanced eruption rates for magmas of  
563 low bulk modulus. Under these conditions, the rapid withdrawal of bubbly magma  
564 inevitably will lead to rapid fragmentation at deep levels in the conduit or even in the  
565 reservoir itself, since the fragmentation threshold is a sensitive function of vesicularity  
566 [*Spieler et al., 2004*].

567       The presence of bubbly magma also will allow efficient syn-eruptive release of  
568 volcanic gas [*Wallace et al., 1995, 1999*]. Silicic magmas, as exemplified by Katmai and  
569 Pinatubo, have a melt phase which is depleted in volatile components such as sulfur, and  
570 a free gas phase which is correspondingly enriched in these components. During  
571 eruptions, the volatiles will be released preferentially at an early stage, due to their  
572 buoyancy and concentration in the upper levels of the magma reservoir. This early release  
573 may be observable by remote sensing methods [*Rose et al., 2000*]. We hypothesize that  
574 many basaltic magmas also contain free gas in the upper parts of their subsurface  
575 plumbing. If so, these sulfur-rich systems may release large amounts of sulfur and other  
576 gases at the beginning of an explosive eruption [e.g., *Rose et al., 2003*].

577

#### 578 **4.4 Modification of Caldera Faults During Subsidence at Fernandina and** 579 **Miyakejima**

580 By contrast with the sudden onset of caldera subsidence at Katmai and Pinatubo,  
 581 collapse at Fernandina and Miyakejima was incremental and progressive. Fernandina and  
 582 Miyakejima provide contrasting insight during caldera subsidence. At Fernandina, the  
 583 patterns of seismic energy release can be grouped into discrete periods. For a given  
 584 period, the interval of time between large earthquakes remained essentially constant, as  
 585 did the magnitude of the earthquakes. The constant time interval implies that a critical  
 586 stress value was attained repeatedly; once this level was reached, it was relieved by  
 587 downward movement of the subsiding caldera block. The similar earthquake magnitudes  
 588 suggest that (a) the block repeatedly subsided the same distance, as calculated above, and  
 589 (b) the stress level returned to a common baseline value. The stress then started to build  
 590 again during the next interval of time as magma continued to drain from the reservoir.

591 Notably at Fernandina, earthquake magnitudes and quiescent intervals both  
 592 decreased abruptly after a period of time, best exemplified at 0851 UTC on 15 June when  
 593 large earthquakes decreased in magnitude from  $M \geq 5$  to  $M 4.7-4.9$  and in spacing from  
 594  $\sim 6$ -hour to  $\sim 4$ -hour intervals. The concurrent decreases in both parameters strongly  
 595 suggest that they are physically linked. The declining time interval can be expressed by  
 596 Equation (1), which can be rewritten as

597

$$598 \quad T = \frac{2V_0(F_s - F_d)}{\kappa\alpha A} \quad (10)$$

599

600

601

602 where  $p' = \kappa\alpha / V_0$ . Here the important parameters are  $V_0$ ,  $\alpha$ ,  $\kappa$ , and  $F_s - F_d$ , which are  
 603 discussed in turn. As the caldera block subsided, the initial volume of the magma  
 604 chamber  $V_0$  was reduced; such a change should manifest itself by a continual decline in  $T$ .

605 This pattern was not observed, however, instead showing discrete periods of constant  $T$   
 606 followed by a decline, as described above. A change in the magma's evacuation rate  $\alpha$   
 607 may also affect the value of  $T$ ; a decrease of  $\alpha$  would increase  $T$ , but the opposite  
 608 behavior is observed. An increase of  $\alpha$  would lower  $T$  and result in greater displacements  
 609 of the subsiding caldera block and thus higher-magnitude earthquakes, but the opposite is  
 610 observed.

611 Increased values of  $\kappa$  would lower  $T$  as shown by Equation (10), implying that the  
 612 magma became less bubbly with time [*Filson et al.*, 1973]. This interesting possibility  
 613 suggests that the initially large subsidence events caused vesicular magma in the upper  
 614 parts of the reservoir to be compressed and pressurized reducing the amount of bubbles,  
 615 to a point where the caldera block stopped moving downward. Between subsidence  
 616 events, the reservoir drained, allowing magma beneath the caldera block to revesiculate  
 617 to an extent where the block again subsided. With time, decreasing volatile contents in  
 618 the magma reduced vesiculation, hence produced less subsidence and lower-magnitude  
 619 earthquakes. The relationship between increasing bulk modulus on the one hand and  
 620 reduced subsidence and smaller-magnitude seismicity on the other hand can be expressed  
 621 quantitatively thus:

622

$$623 \quad z = \frac{2V_0(F_s - F_d)}{\kappa A^2} \quad (11)$$

624  
625  
626

627 The shorter intervals between subsidence events may imply that evacuation rates  
 628 increased over time.

629           A second possibility is that  $F_s - F_d$  declined during magma withdrawal and  
630 subsidence, causing  $T$  to decrease, as suggested originally by *Filson et al.* [1973] and  
631 examined recently by *Kobayashi et al.* [2003] at Miyakejima. Essentially, a lower critical  
632 stress threshold was reached sooner, and the block subsided. For a given evacuation rate,  
633 the shortened time interval between subsidence events resulted in smaller amounts of  
634 downward displacement of the caldera block. As a result, earthquake magnitudes also  
635 decreased. It appears that the friction forces resisting downward movement of the caldera  
636 block decreased with time in a stepwise fashion. This weakening process appears to have  
637 occurred at discrete intervals rather than as a continuous process.

638           A final view is that the caldera faults were inward dipping. As magma drained  
639 from the reservoir initially, the extent of collapse was comparatively large. As the magma  
640 continued to drain, however, the ability of the caldera block to subside diminished  
641 progressively due to the constricting faults. With time, the block became wedged between  
642 the faults, and subsidence ceased. This hypothesis is difficult to evaluate, as we have no  
643 direct evidence regarding the configuration of the caldera faults.

644           We can identify a similar temporal change of magnitude and time interval in the  
645 individual VLP events of Miyakejima, which provides complementary information for  
646 the understanding of frictional control. *Kobayashi et al.* [2003] have studied sequences of  
647 small-amplitude earthquakes, especially in the events at the beginning of the VLP activity,  
648 which were observed to occur about an hour before the appearance of a VLP signal.  
649 Initially, time intervals between these precursor earthquakes exhibited progressive and  
650 linear declines, while the earthquake amplitudes remained constant until near the end of a  
651 sequence when the amplitudes declined precipitously. To explain these patterns,

652 *Kobayashi et al.* [2003] use an asperity model where the caldera piston is strongly  
653 coupled to the country rock by means of “asperites”. The repeated earthquakes of similar  
654 amplitude represent the progressive breaking of individual asperites which maintain  
655 constant strength. As asperites break, the stress level returns to a baseline which then  
656 increases more rapidly with time, since there are progressively fewer asperites holding  
657 the block stationary against the country rock. Eventually, all asperites are broken, the  
658 critical stress level declines rapidly to the baseline value, and the block starts to move.  
659 This view of an individual subsidence event at Miyakejima shares similarities with the  
660 sequence of subsidence events at Fernandina.

661       When examining the overall activity at Miyakejima, however, the temporal trends  
662 provide a contrasting case to Fernandina. At Day ~500 about halfway through the events  
663 of 2000 (Fig. 3), the time interval between successive VLP events increased, as did the  
664 magnitudes and energies of individual VLP signals. This interesting observation is  
665 exactly opposite to that seen for Fernandina. The seismic energy of a VLP signal is  
666 related to an enhanced internal pressure of the magma chamber  $\Delta p$ , which can be  
667 rewritten as  $2V_0(F_s - F_d)/A$ . Assuming that the  $A$  and  $V_0$  parameters remain constant, the  
668 friction parameter  $(F_s - F_d)$  controls the temporal features in magnitude and time interval  
669 simultaneously, suggesting that the effective friction on the caldera faults may have  
670 increased in early August 2000. If this interpretation is correct, then a longer time  
671 interval was required to reach the point of failure. If the magma evacuation rate remained  
672 constant, the longer time interval implies that a greater amount of magma was drained  
673 from the reservoir than previously occurred. Hence, the caldera block was able to fall  
674 further during an individual subsidence event, producing a large-magnitude VLP signal.

675 In summary, for both Fernandina and Miyakejima, friction acting on the conduit wall  
676 may play a pivotal role for the process of incremental subsidence of the piston.

677

678

## 679 **5. Conclusions**

680 The principal conclusions from this work are the following:

- 681 1. Caldera collapse at Katmai and Pinatubo occurred en masse at a comparatively late  
682 stage in the course of the eruption, while subsidence at Fernandina and Miyakejima  
683 proceeded incrementally. The en masse collapse was caused by the caldera block  
684 subsiding in response to magma evacuation. By contrast, the incremental collapse  
685 observed at the basaltic calderas may have resulted from the periodically subsiding  
686 block forcefully pushing magma out of the reservoir.
- 687 2. During its evacuation, the magma in the reservoirs beneath Katmai and Pinatubo  
688 possessed significant porosity and compressibility. Due to its compressibility and low  
689 viscosity, the rhyolite magma at Katmai was easily extracted and erupted, leading to  
690 significant underpressures prior to caldera subsidence.
- 691 3. At Katmai, changes in magma rheology appear to have played an important role in  
692 magma withdrawal and timing of collapse. The development of underpressure may be  
693 controlled by a delicate balance among certain parameters including the evacuation  
694 rate of the magma, its bulk modulus, and its crystal content.
- 695 4. Incremental collapse at Fernandina and Miyakejima reveals contrasting behavior  
696 which is probably related to modification of the caldera fault systems over the course  
697 of protracted subsidence.

698 5. The amount of extractable and eruptable magma present in the reservoir determines,  
699 at least in part, the degree of underpressure in the reservoir, the evacuation rate of the  
700 magma, and the timing and style of caldera collapse. Such magmas possess low  
701 viscosities, small amounts of crystals, and substantial amounts of bubbles.

702

703 At Katmai and Pinatubo, magma discharge rates did not appear to increase when the  
704 bulk of subsidence occurred, since most of the ignimbrites had already been erupted  
705 before the major collapse episodes were initiated. Intracaldera ponding of ignimbrite does  
706 not appear to be significant at either volcano. For all four volcanoes studied here, the  
707 subsiding caldera blocks appear to have behaved coherently, either as pistons or as en  
708 masse subsidence. Aspect ratios of the caldera blocks for Katmai, Pinatubo, Miyakejima,  
709 and possibly Fernandina as well, may exceed those of larger caldera systems, where roof  
710 blocks may resemble thin plates. For these large systems, collapse may occur more  
711 incrementally and at an earlier stage due to the smaller aspect ratio. Incremental collapse  
712 promotes progressive ponding of ignimbrite, increasing the lithostatic load of the  
713 subsiding block. Thus, incremental collapse may result in an eruption style quite different  
714 from that associated with en masse collapse.

715

716 **Acknowledgements.** The starting point for this work began after reading Wes Hildreth  
717 and Judy Fierstein's fascinating paper on Katmai which they published in 2000. Events at  
718 Miyakejima volcano in 2000 also helped influence some of the ideas developed during  
719 our research. Comments by Ben Kennedy on an earlier version of the manuscript  
720 measurably improved the paper. Experimental work by Richard Sunde and Valérie



721 Frechette helped clarify some points regarding the role of magma evacuation rate on  
722 caldera collapse. Formal reviews by Joan Martí and Hiroyuki Kumagai and comments by  
723 Associate Editor Michael Ryan were inciteful, forcing us to rethink some of our ideas and  
724 conclusions. This study was supported by an operating grant from the Natural Sciences  
725 and Engineering Research Council of Canada and a team grant from Le Fonds québécois  
726 de la recherche sur la nature et les technologies.

727

## 728 **References**

- 729 Abe, K. (1992), Seismicity of the caldera-making eruption of Mount Katmai, Alaska in  
730 1912, *Bull. Seismol. Soc. Am.*, 82, 175-191.
- 731 Bacon, C.R., and T. H. Druitt (1988), Compositional evolution of the zoned calcalkaline  
732 magma chamber of Mount Mazama, Crater Lake, Oregon, *Contrib. Mineral. Petrol.*,  
733 98, 224-256.
- 734 Bautista, B. C., Ma. L. P. Bautista, R. S. Stein, E. S. Barcelona, R. S. Punongbayan, E. P.  
735 Laguerta, A. R. Rasdas, G. Ambubuyog, and E. Q. Amin (1996), Relationship of  
736 regional and local structures to Mount Pinatubo activity, in *Fire and Mud: Eruptions  
737 and Lahars of Mount Pinatubo, Philippines*, edited by C. G. Newhall and R. S.  
738 Punongbayan, pp. 351-370, Philippine Institute of Volcanology and Seismology,  
739 Quezon City, and University of Washington Press, Seattle and London.
- 740 Byerlee, J. D. (1978), Friction of rocks, *Pure Appl. Geophys.*, 116, 615-626.
- 741 Coombs, M. L., and J. E. Gardner (2001), Shallow-storage conditions for the rhyolite of  
742 the 1912 eruption at Novarupta, Alaska, *Geology*, 29, 775-778.

- 743 Cornet, F. H., and B. Valette (1984), In situ stress determination from hydraulic injection  
744 test data, *J. Geophys. Res.*, *89*, 11527-11537.
- 745 Cowee, C., J. F. Larsen, H. Geutschow, J. Eichelberger, A. Kent, and I. Hutcheon (1999),  
746 Melt inclusion textures and volatile compositions from Novarupta Dome, Katmai  
747 National Park, Alaska, *Eos Trans. AGU*, *80*, Spring Meet. Suppl., S353.
- 748 Druitt, T.H., and R. S. J. Sparks (1984), On the formation of calderas during ignimbrite  
749 eruptions, *Nature*, *310*, 679-681.
- 750 Druitt, T. H., and C. R. Bacon C.R. (1986), Lithic breccia and ignimbrite erupted during  
751 the collapse of Crater Lake Caldera, Oregon, *J. Volcanol. Geotherm. Res.*, *29*, 1-32.
- 752 Filson, J., T. Simkin, and L.-K. Leu (1973), Seismicity of a caldera collapse: Galapagos  
753 Islands 1968, *J. Geophys. Res.*, *78*, 8591-8622.
- 754 Folch, A., and J. Martí (1998), The generation of overpressure in felsic magma chambers  
755 by replenishment, *Earth Planet. Sci. Lett.*, *163*, 301-314.
- 756 Furuya M., S. Ohkubo, W. Sun, Y. Tanaka, J. Oikawa, and H. Watanabe (2003),  
757 Spatiotemporal gravity changes at Miyakejima volcano, Japan: caldera collapse,  
758 explosive eruptions and magma movement, *J. Geophys. Res.*, *108*,  
759 10.1029/2002JB001989
- 760 Geshi, N., T. Shimano, T. Chiba, and S. Nakada (2002), Caldera collapse during the 2000  
761 eruption of Miyakejima volcano, Japan, *Bull. Volcanol.*, *64*, 55-68.
- 762 Hess, K.-U., and D. B. Dingwell (1996), Viscosities of hydrous leucogranitic melts: a  
763 non-Arrhenian model, *Am. Mineral.*, *81*, 1297-1300.

- 764 Hildreth, W. (2004), Volcanological perspectives on Long Valley, Mammoth Mountain,  
765 and Mono Craters: several contiguous but discrete systems, *J. Volcanol. Geotherm.*  
766 *Res.*, 136, 169-198.
- 767 Hildreth, W., and J. Fierstein (2000), Katmai volcanic cluster and the great eruption of  
768 1912, *Geol. Soc. Am. Bull.*, 112, 1594-1620.
- 769 Hoblitt, R. P., E. W. Wolfe, W. E. Scott, M. R. Couchman, J. S. Pallister, and D. Javier  
770 (1996), The preclimactic eruptions of Mount Pinatubo, June 1991, in *Fire and Mud:*  
771 *Eruptions and Lahars of Mount Pinatubo, Philippines*, edited by C. G. Newhall and R.  
772 S. Punongbayan, pp. 457-511, Philippine Institute of Volcanology and Seismology,  
773 Quezon City, and University of Washington Press, Seattle and London.
- 774 Huppert, H. E., and A. W. Woods (2002), The role of volatiles in magma chamber  
775 dynamics, *Nature*, 420, 493-495.
- 776 Irwan, M., F. Kimata, N. Fujii, S. Nakano, H. Watanabe, S. Sakai, M. Ukawa, E. Fujita,  
777 and K. Kawai (2003), Rapid ground deformation of the Miyakejima volcano on 26-27  
778 June 2000 detected by kinematic GPS analysis, *Earth Planets Space*, 55, e13-e16.
- 779 Jones, J. W., and C. G. Newhall (1996), Preruption and posteruption digital-terrain  
780 models of Mount Pinatubo, in *Fire and Mud: Eruptions and Lahars of Mount Pinatubo,*  
781 *Philippines*, edited by C. G. Newhall and R. S. Punongbayan, pp. 571-582, Philippine  
782 Institute of Volcanology and Seismology, Quezon City, and University of Washington  
783 Press, Seattle and London.
- 784 Kaneko, T., A. Yasuda, T. Shimano, S. Nakada, T. Fujii, T. Kanazawa, A. Nishizawa,  
785 and Y. Matsumoto (2005), Submarine flank eruption preceding caldera subsidence  
786 during the 2000 eruption of Miyakejima volcano, Japan, *Bull. Volcanol.*, 67, 243-253.

- 787 Kazahaya, K., Y. Nakahori, H. Mori, H. Iino, M. Miyashita, J. Hirabayashi, H.  
788 Shinohara, K. Uto, and M. Odai (2004), Gigantic SO<sub>2</sub> emission from Miyakejima  
789 volcano, Japan, caused by caldera collapse, *Geology*, 32, 425-428.
- 790 Kennedy, B., and J. Stix (2003), Styles and mechanisms of caldera collapse, *Geosci.*  
791 *Can.*, 30, 59-72.
- 792 Kennedy, B., and J. Stix (2007), Magmatic processes associated with caldera collapse at  
793 Ossipee ring dyke, New Hampshire, *Geol. Soc. Am. Bull.*, 119, 3-17.

- 794 Kennedy, B., J. Stix, J. W. Vallance, Y. Lavallée, and M.-A. Longpré (2004), Controls on  
795 caldera structure: results from analogue sandbox modeling, *Geol. Soc. Am. Bull.*, *116*,  
796 515-524.
- 797 Khitarov, N. I., Ye. B. Lebedev, A. B. Slutskin, A. M. Dorfman, I. A. Soldatov, and N. I.  
798 Revin (1976), The pressure dependence of the viscosity of basalt melts, *Geochem. Intl.*,  
799 *13*(5), 126-133.
- 800 Kikuchi, M., Y. Yamanaka, and K. Koketsu (2001), Source process of the long-period  
801 seismic pulses associated with the 2000 eruption of Miyake-jima volcano, and its  
802 implications, *J. Geogr.*, *110*, 204-216.
- 803 Kobayashi, T., T. Ohminato, and Y. Ida (2003), Earthquake series preceding very long  
804 period seismic signals, observed during the 2000 Miyakejima volcanic activity,  
805 *Geophys. Res. Lett.*, *30*(8), 1423, doi:10.1029/2002GL016631.
- 806 Koyaguchi, T., and M. Ohno (2001), Reconstruction of eruption column dynamics on the  
807 basis of grain size of tephra fall deposits 2. Application to the Pinatubo 1991 eruption,  
808 *J. Geophys. Res.*, *106*, 6513-6533.
- 809 Kumagai, H., T. Ohminato, M. Nakano, M. Ooi, A. Kubo, H. Inoue, and J. Oikawa  
810 (2001), Very-long-period seismic signals and caldera formation at Miyake Island,  
811 Japan, *Science*, *293*, 687-690.
- 812 Lavallée, Y., K.-U. Hess, B. Cordonnier, and D. B. Dingwell (2007), Non-Newtonian  
813 rheological law for highly crystalline dome lavas, *Geology*, *35*, 843-846.
- 814 Legros, F., K. Kelfoun, and J. Martí (2000), The influence of conduit geometry on the  
815 dynamics of caldera-forming eruptions, *Earth Planet. Sci. Lett.*, *179*, 53-61.

- 816 Lowenstern, J. B. (1993), Evidence for a copper-bearing fluid in magma erupted at the  
817 Valley of Ten Thousand Smokes, Alaska, *Contrib. Mineral. Petrol.*, *114*, 409-421.
- 818 Martí, J., A. Folch, A. Neri, and G. Macedonio (2000), Pressure evolution during  
819 explosive caldera-forming eruptions, *Earth Planet. Sci. Lett.*, *175*, 275-287.
- 820 Mori, J., D. Eberhart-Phillips, and D. H. Harlow (1996a), Three-dimensional velocity  
821 structure at Mount Pinatubo: resolving magma bodies and earthquake hypocenters, in  
822 *Fire and Mud: Eruptions and Lahars of Mount Pinatubo, Philippines*, edited by C. G.  
823 Newhall and R. S. Punongbayan, pp. 371-382, Philippine Institute of Volcanology and  
824 Seismology, Quezon City, and University of Washington Press, Seattle and London.
- 825 Mori, J., R. A. White, D. H. Harlow, P. Okubo, J. A. Power, R. P. Hoblitt, E. P. Laguerta,  
826 A. Lanuza, and B. C. Bautista (1996b), Volcanic earthquakes following the 1991  
827 climactic eruption of Mount Pinatubo: strong seismicity during a waning eruption, in  
828 *Fire and Mud: Eruptions and Lahars of Mount Pinatubo, Philippines*, edited by C. G.  
829 Newhall and R. S. Punongbayan, pp. 339-350, Philippine Institute of Volcanology and  
830 Seismology, Quezon City, and University of Washington Press, Seattle and London.
- 831 Nakada, S., M. Nagai, T. Kaneko, A. Nozawa, and K. Suzuki-Kimata (2005),  
832 Chronology and products of the 2000 eruption of Miyakejima volcano, Japan, *Bull.*  
833 *Volcanol.*, *67*, 205-218.
- 834 Roche, O., and T. H. Druitt (2001), Onset of caldera collapse during ignimbrite eruptions,  
835 *Earth Planet. Sci. Lett.*, *191*, 191-202.
- 836 Roche, O., T. H. Druitt, and O. Merle (2000), Experimental study of caldera formation, *J.*  
837 *Geophys. Res.*, *105*, 395-416.

- 838 Rose, W. I., G. J. S. Bluth, and G. G. J. Ernst (2000), Integrating retrievals of volcanic  
839 cloud characteristics from satellite remote sensors: a summary, *Phil. Trans. Royal. Soc.*  
840 *Edinburgh, A358*, 1585-1606.
- 841 Rose, W. I., Y. Gu, I. M. Watson, T. Yu, G. J. S. Bluth, A. J. Prata, A. J. Krueger, N.  
842 Krotkov, S. Carn, M. D. Fromm, D. E. Hunton, G. G. J. Ernst, A. A. Viggiano, T. M.  
843 Miller, J. O. Balenthin, J. M. Reeves, J. C. Wilson, B. E. Anderson, and D. E. Flittner  
844 (2003), The February-March 2000 eruption of Hekla, Iceland from a satellite  
845 perspective, *Am. Geophys. Union Geophys. Mon.*, 139, 107-132.
- 846 Rutherford, M. J., and J. D. Devine (1996), Preeruption pressure-temperature conditions  
847 and volatiles in the 1991 dacitic magma of Mount Pinatubo, in *Fire and Mud: Eruptions*  
848 *and Lahars of Mount Pinatubo, Philippines*, edited by C. G. Newhall and R. S.  
849 Punongbayan, pp. 751-766, Philippine Institute of Volcanology and Seismology,  
850 Quezon City, and University of Washington Press, Seattle and London.
- 851 Scaillet, B., F. Holtz, and M. Pichavant (1998), Phase equilibrium constraints on the  
852 viscosity of silicic magmas, *J. Geophys. Res.*, 103, 27257-27266.
- 853 Scott, W. E., R. P. Hoblitt, R. C. Torres, S. Self, Ma. M. L. Martinez, and T. Nillos, Jr.  
854 (1996) Pyroclastic flows of the June 15, 1991, climactic eruption of Mount Pinatubo, in  
855 *Fire and Mud: Eruptions and Lahars of Mount Pinatubo, Philippines*, edited by C. G.  
856 Newhall and R. S. Punongbayan, pp. 545-570, Philippine Institute of Volcanology and  
857 Seismology, Quezon City, and University of Washington Press, Seattle and London.
- 858 Simkin, T., and K. A. Howard (1970), Caldera collapse in the Galápagos Islands, 1968,  
859 *Science*, 169, 429-437.

- 860 Smith, R.L. (1979), Ash-flow magmatism, in *Ash-Flow Tuffs, Geol. Soc. Am. Spec. Pap.*,  
861 *180*, edited by C. E. Chapin and W. E. Elston, pp. 5-27.
- 862 Spieler, O., D. B. Dingwell, B. Scheu, J. Taddeucci, B. Kennedy, and U. Kueppers  
863 (2004), The fragmentation threshold of pyroclastic rocks, *Earth Planet. Sci. Lett.*, *226*,  
864 139-148.
- 865 Stein, D. J., and F. J. Spera (2002), Shear viscosity of rhyolite-vapor emulsions at  
866 magmatic temperatures by concentric cylinder rheometry, *J. Volcanol. Geotherm. Res.*,  
867 *113*, 243-258.
- 868 Stix, J., and M. P. Gorton (1993), Replenishment and crystallization in epicontinental  
869 silicic magma chambers: Evidence from the Bandelier magmatic system. *J. Volcanol.*  
870 *Geotherm. Res.*, *55*, 201-215.
- 871 Sunde, R., J. Stix, and B. Kennedy (2004), The effect of eruption rate on caldera  
872 structure: analogue experiments, *Eos Trans. AGU*, *85*(17), Jt. Assem. Suppl., Abstract  
873 V43A-17.
- 874 Ueda, H., E. Fujita, M. Ukawa, E. Yamamoto, M. Irwan, and F. Kimata (2005), Magma  
875 intrusion and discharge process at the initial stage of the 2000 activity of Miyakejima,  
876 central Japan, inferred from tilt and GPS data, *Geophys. J. Int.*, *161*, 891-906.
- 877 Uhira, K., T. Baba, H. Mori, H. Katayama, and N. Hamada (2005), Earthquake swarms  
878 preceding the 2000 eruption of Miyakejima volcano, Japan, *Bull. Volcanol.*, *67*, 219-  
879 230.
- 880 Ukawa M., E. Fujita, E. Yamamoto, Y. Okada, and M. Kikuchi (2000), The 2000  
881 Miyakejima eruption: Crustal deformation and earthquakes observed by the NIED  
882 Miyakejima observation network, *Earth Planets Space*, *52*, xix-xxvi.



- 883 Wallace, P., and T. M. Gerlach (1994), Magmatic vapor source for sulfur dioxide  
884 released during volcanic eruptions: evidence from Mount Pinatubo, *Science*, 265, 497-  
885 499.
- 886 Wallace, P. J., A. T. Anderson Jr., and A. M. Davis (1995), Quantification of pre-eruptive  
887 exsolved gas contents in silicic magmas, *Nature*, 377, 612-616.
- 888 Wallace, P. J., Anderson Jr., and A. M. Davis (1999), Gradients in H<sub>2</sub>O, CO<sub>2</sub>, and  
889 exsolved gas in a large-volume silicic magma system: Interpreting the record preserved  
890 in melt inclusions from the Bishop Tuff, *J. Geophys. Res.*, 104, 20097-20122.
- 891 Westrich, H. R., J. C. Eichelberger, and R. L. Hervig (1991), Degassing of the 1912  
892 Katmai magmas: *Geophys. Res. Lett.*, 18, 1561-1564.
- 893 Yamaoka, K., M. Kawamura, F. Kimata, N. Fujii, and T. Kudo (2005), Dike intrusion  
894 associated with the 2000 eruption of Miyakejima volcano, Japan, *Bull. Volcanol.*, 67,  
895 231-242.
- 896

896 **Figure captions**

897

898 Figure 1. Plot of cumulative energy released by large earthquakes during the (a) Katmai  
899 1912, (b) Pinatubo 1991, and (c) Fernandina 1968 caldera-forming eruptions. The  
900 steplike patterns of energy released at Katmai and Pinatubo contrast with the progressive  
901 trend seen at Fernandina. Note the different time and energy scales for the three events.

902 Energies were calculated as  $\log E = 1.96 M + 2.05$  where  $E$  is the energy in Joules and  $M$   
903 the magnitude of the earthquake. Sources of data as follows: Katmai, *Abe* [1992];

904 Pinatubo, National Earthquake Information Center, <http://earthquake.usgs.gov/regional/neic/>;

905 Fernandina, *Filson et al.* [1973].

906

907 Figure 2. Cumulative energy plots for (a) Katmai 1912 and (b) Pinatubo 1991, in which  
908 the diagrams have been made non-dimensional. Time plotted on the x axis is normalized  
909 relative to the duration of the climactic eruptions; for Katmai, the duration was 60 hours,  
910 while for Pinatubo the duration was ~8.8 hours. Cumulative energy released by large  
911 earthquakes is normalized relative to the total amount of cumulative energy liberated  
912 during and immediately after the climactic eruptions.

913

914 Figure 3. Plot of energies of VLP events, both individual and cumulative, recorded at  
915 Miyakejima in July and August 2000. Using the relationship between the seismic energy  
916 (Joules) and seismic moment (Nm)  $\log E_s = \log M_0 - 4.3$ , we can evaluate the released  
917 seismic energy of each VLP event. In this calculation, we used the seismic moment of 39  
918 VLP signals listed in *Kikuchi et al.* [2001] and obtained the values for  $M_0$  from their

919 Figure 9. Also shown are caldera volumes plotted as a function of time and shown as  
920 solid circles; data from *Geshi et al.* [2002].

921

922 Figure 4. Schematic diagram of piston subsidence (a) prior to caldera collapse (e.g.,  
923 Katmai, Pinatubo) and (b) after an increment of collapse (e.g., Fernandina, Miyakejima).

924 The aspect ratio is  $R = H / D$ . See Table 2 for symbology and text for equations.

925

926 Figure 5. Magma underpressure plotted as a function of bulk modulus of the magma for  
927 the Katmai, Pinatubo, and Fernandina eruptions. Typical rock shear strengths are also  
928 shown. See text for discussion.

929

930 Figure 6. Caldera subsidence plotted against evacuation rate. The amount of  
931 displacement is calculated using Equation (8). A range of evacuation rates is used based  
932 on published values of volumetric eruption rates. (a) Katmai 1912; (b) Pinatubo 1991.

933

934 Figure 7. Caldera subsidence at Fernandina as a function of (a) evacuation rate of magma  
935 and (b) the time interval before subsidence. The amount of displacement is calculated  
936 using Equation (8).

937

938

939

940

941

942

943

944

945  
946  
947  
948  
949  
950  
951  
952  
953  
954  
955  
956  
957  
958  
959  
960  
961  
962  
963  
964  
965  
966  
967  
968  
969  
970  
971  
972  
973  
974  
975  
976  
977  
978  
979  
980  
981  
982  
983  
984  
985  
986  
987  
988  
989  
990

Table 1. Input values for modeling

| Parameter  | Katmai                                 | Pinatubo                               | Fernandina                             | Miyakejima                             |
|--|--|--|--|--|
| Aspect ratio of caldera block, $R$ (dimensionless)                           | 2.0                                    | 2.4                                    | 0.31                                   | 1.9 - 3.8                              |
| Initial volume of magma reservoir, $V_0$ ( $m^3$ )                           | $1.3 \times 10^{10}$                   | $5.0 \times 10^9$                      | $2.2 \times 10^9$                      | $3.7 \times 10^{10}$                   |
| Cross-sectional area of base of caldera block, $A$ ( $m^2$ )                 | $4.0 \times 10^6$                      | $4.9 \times 10^6$                      | $8.0 \times 10^6$                      | $2.0 \times 10^6$                      |
| Duration of magma evacuation before caldera block begins to subside, $T$ (s) | 117,360                                | 17,953                                 | 21,600                                 | 43,200 to 86,400                       |
| Magma evacuation rate, $\alpha$ ( $m^3 s^{-1}$ )                             | $2.8 \times 10^4$ to $2.2 \times 10^5$ | $1.2 \times 10^5$ to $3.6 \times 10^5$ | $3.0 \times 10^3$ to $6.7 \times 10^3$ | $4.5 \times 10^1$ to $1.7 \times 10^2$ |

Sources of data: Katmai, *Hildreth and Fierstein* [2000]; Pinatubo, *Hoblitt et al.* [1996], *Koyaguchi and Ohno* [2001], *Mori et al.* [1996a, 1996b], *Scott et al.* [1996]; Fernandina, *Simkin and Howard* [1970], *Filson et al.* [1973]; Miyakejima, *Kumagai et al.* [2001], *Geshi et al.* [2002], *Kobayashi et al.* [2003], *Irwan et al.* [2003], *Ueda et al.* [2005].

991  
992 Table 2. Symbols used in equations  
993  
994  
995  
996

|      |              |  |
|------|--------------|--|
| 997  | $E$          | energy of volcanotectonic earthquake (J)   |
| 998  | $E_s$        | energy of VLP event (J)  |
| 999  | $M$          | magnitude of volcanotectonic earthquake  |
| 1000 | $M_0$        | seismic moment of VLP event (N m)  |
| 1001 | $A$          | cross-sectional area at the base of caldera block (m <sup>2</sup> )                |
| 1002 | $H$          | thickness of caldera block (m)   |
| 1003 | $D$          | diameter of caldera block (m)  |
| 1004 | $R$          | aspect ratio of caldera block, $H/D$ (dimensionless)                               |
| 1005 | $z$          | displacement of caldera block (m)  |
| 1006 | $V_o$        | initial volume of magma chamber prior to caldera subsidence (m <sup>3</sup> )      |
| 1007 | $\Delta V$   | change in volume (m <sup>3</sup> )   |
| 1008 | $T$          | time between initiation of magma chamber evacuation and downward movement          |
| 1009 |              | of caldera block (s)   |
| 1010 | $\alpha$     | evacuation rate of magma (m <sup>3</sup> s <sup>-1</sup> )                         |
| 1011 | $F_s$        | static friction (N)  |
| 1012 | $F_d$        | dynamic friction (N)   |
| 1013 | $p_o$        | original pressure in magma chamber (Pa)  |
| 1014 | $p$          | pressure increase in magma chamber from downward movement of caldera block         |
| 1015 |              | (Pa)   |
| 1016 | $p'T$        | underpressure in magma chamber (Pa)  |
| 1017 | $p'T_{crit}$ | critical magma underpressure to cause failure of caldera roof and initiate caldera |
| 1018 |              | collapse (Pa)  |
| 1019 | $p'$         | rate of pressure decrease in magma chamber (Pa s <sup>-1</sup> )                   |
| 1020 | $p_1$        | re-equilibrated pressure in magma chamber (Pa)                                     |
| 1021 | $p_{lith}$   | lithostatic pressure (Pa)  |
| 1022 | $\Delta p$   | pressure difference (Pa)   |
| 1023 | $\kappa$     | bulk modulus of magma (Pa)   |
| 1024 | $\tau_c$     | critical shear stress for failure of caldera block (Pa)                            |
| 1025 | $\tau_o$     | cohesion of caldera block (Pa)   |
| 1026 | $\sigma_n$   | mean stress normal to the plane of failure (Pa)                                    |
| 1027 | $\mu$        | coefficient of internal friction of the caldera block (dimensionless)              |
| 1028 | $k$          | constant ( $\sim 0.6$ ) (dimensionless)  |
| 1029 | $\rho_r$     | density of caldera block (kg m <sup>-3</sup> )                                     |
| 1030 | $g$          | acceleration due to gravity (m s <sup>-2</sup> )                                   |
| 1031 |              |  |
| 1032 |              |  |
| 1033 |              |  |
| 1034 |              |  |
| 1035 |              |  |
| 1036 |              |  |

1037  
 1038  
 1039  
 1040  
 1041  
 1042  
 1043  
 1044  
 1045  
 1046  
 1047  
 1048  
 1049  
 1050  
 1051  
 1052  
 1053  
 1054  
 1055  
 1056  
 1057  
 1058  
 1059  
 1060  
 1061  
 1062  
 1063  
 1064  
 1065  
 1066

Table 3. Downward displacement of the caldera block as a function of magma evacuation rate.

| Parameter  | Katmai            |                   | Pinatubo          |                   |
|--|-------------------|-------------------|-------------------|-------------------|
|  | Minimum           | Maximum           | Minimum           | Maximum           |
| Observed evacuation rate of magma ( $\text{m}^3 \text{s}^{-1}$ ) | $2.8 \times 10^4$ | $2.2 \times 10^5$ | $1.2 \times 10^5$ | $3.6 \times 10^5$ |
| Calculated displacement of the caldera block (m)                 | 822               | 6484              | 440               | 1320              |
| Observed surface displacement of the caldera block (m)           | 1200-1300         |                   | ~900              |                   |

Sources of data: Katmai, *Hildreth and Fierstein* [2000]; Pinatubo, *Jones and Newhall* [1996], *Koyaguchi and Ohno* [2001], *Scott et al.* [1996].

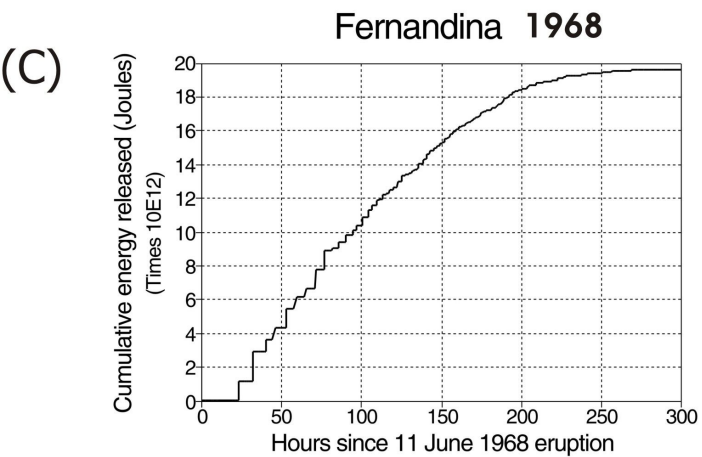
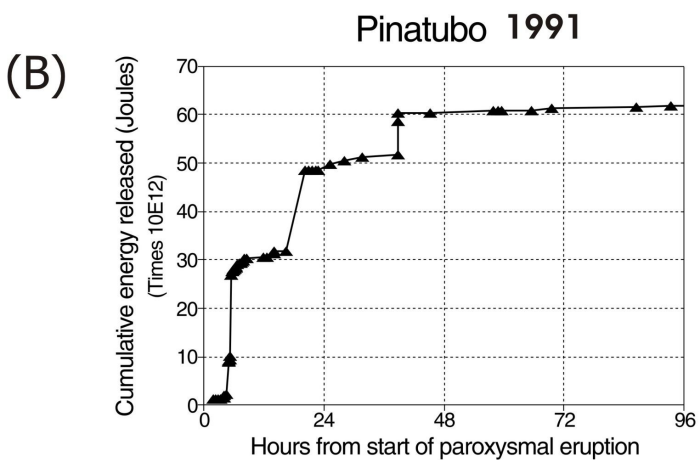
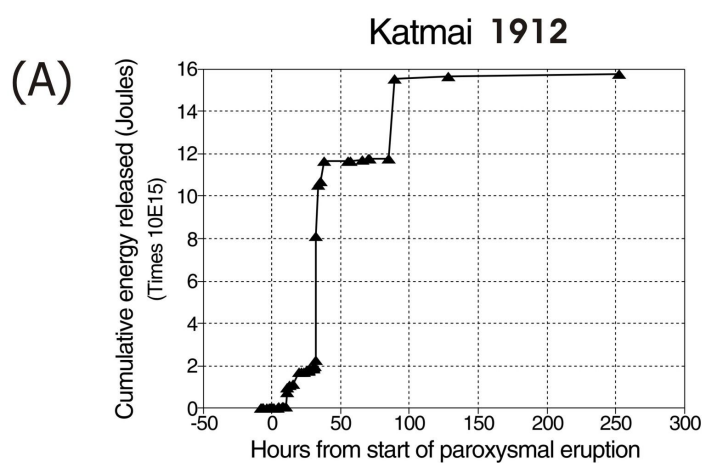
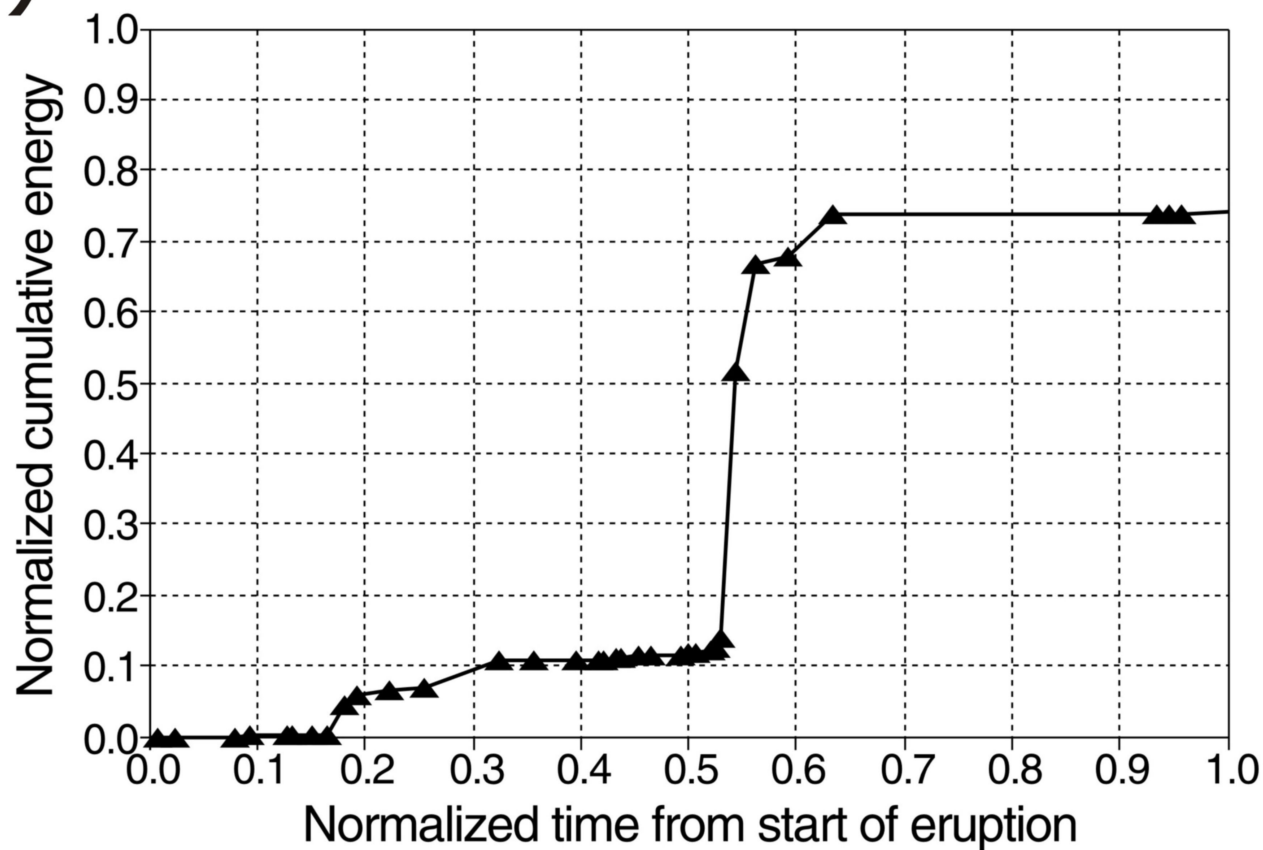
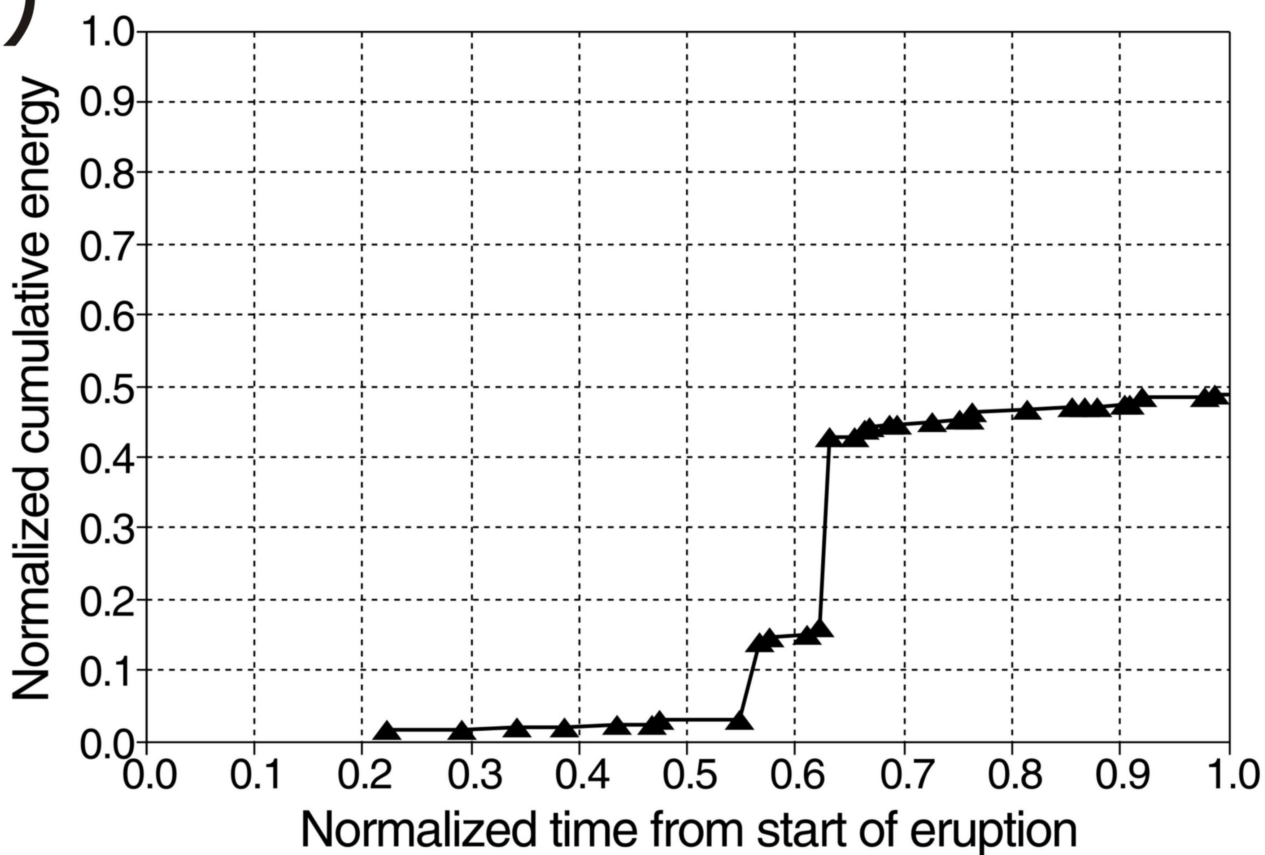
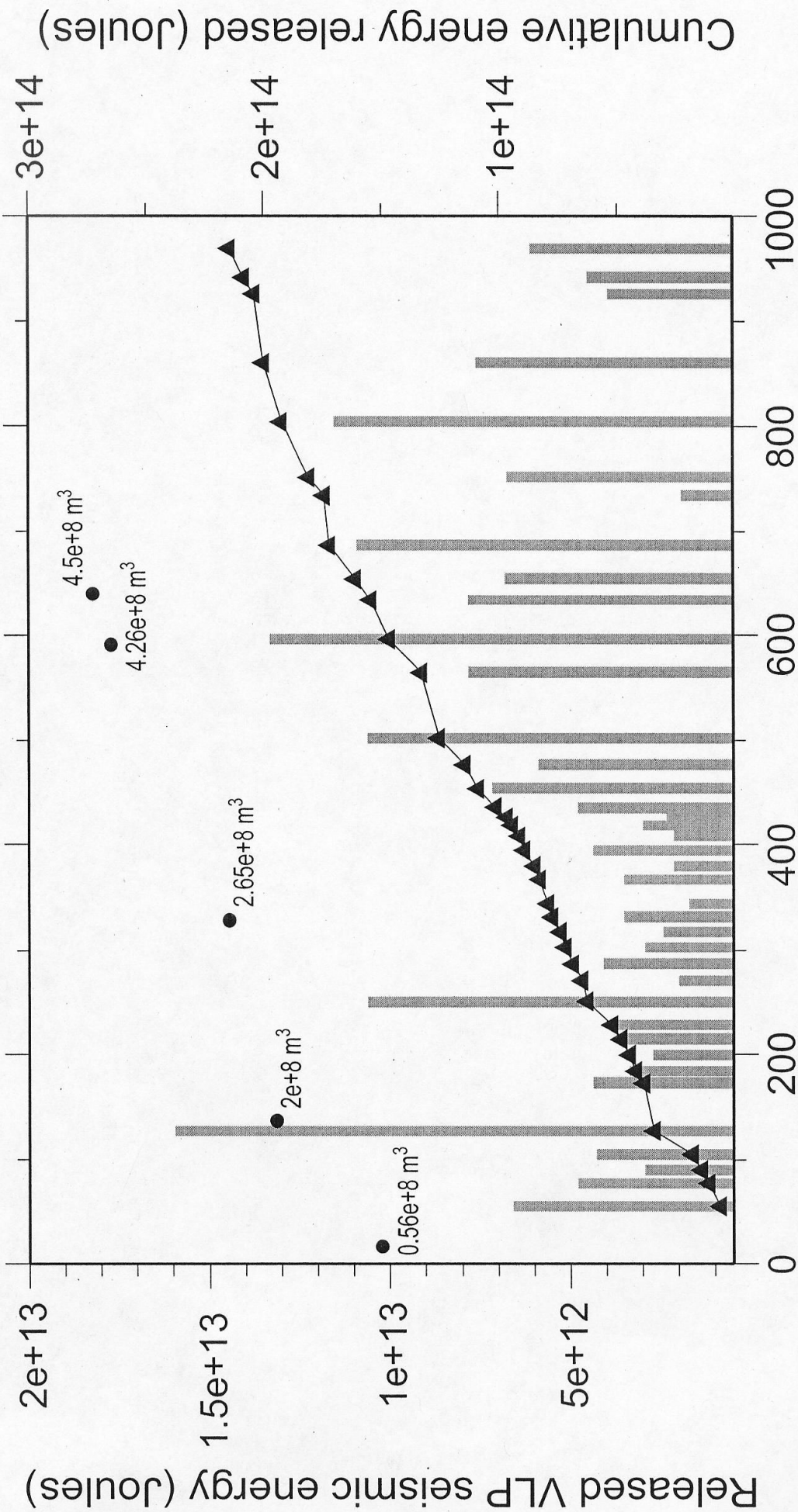


Fig. 1

**(A)****Katmai****(B)****Pinatubo**

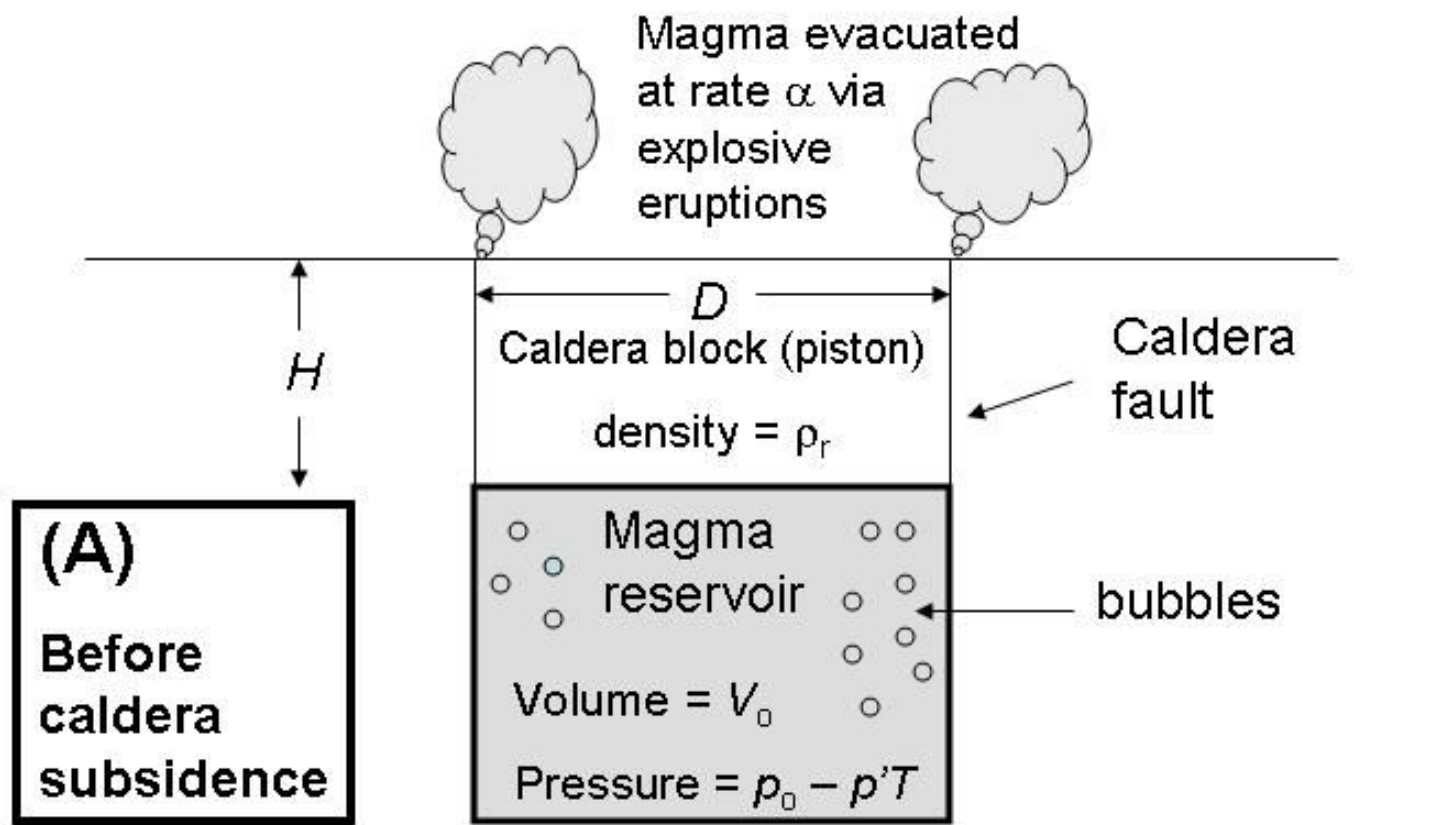


# VLP Seismic Energy



Hours since 8 July 2000 eruption

Fig. 3



Caldera subsidence is initiated when  $p'T_{crit}A = 2(F_s - F_d)$

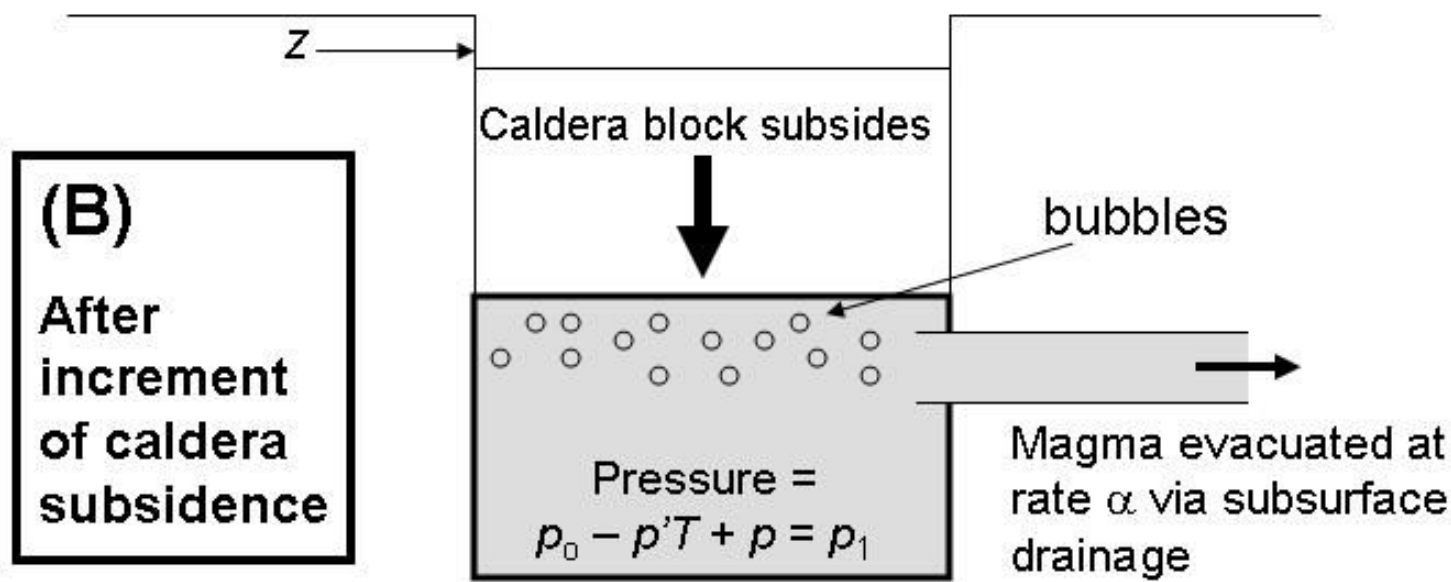


Fig. 4

# Underpressure

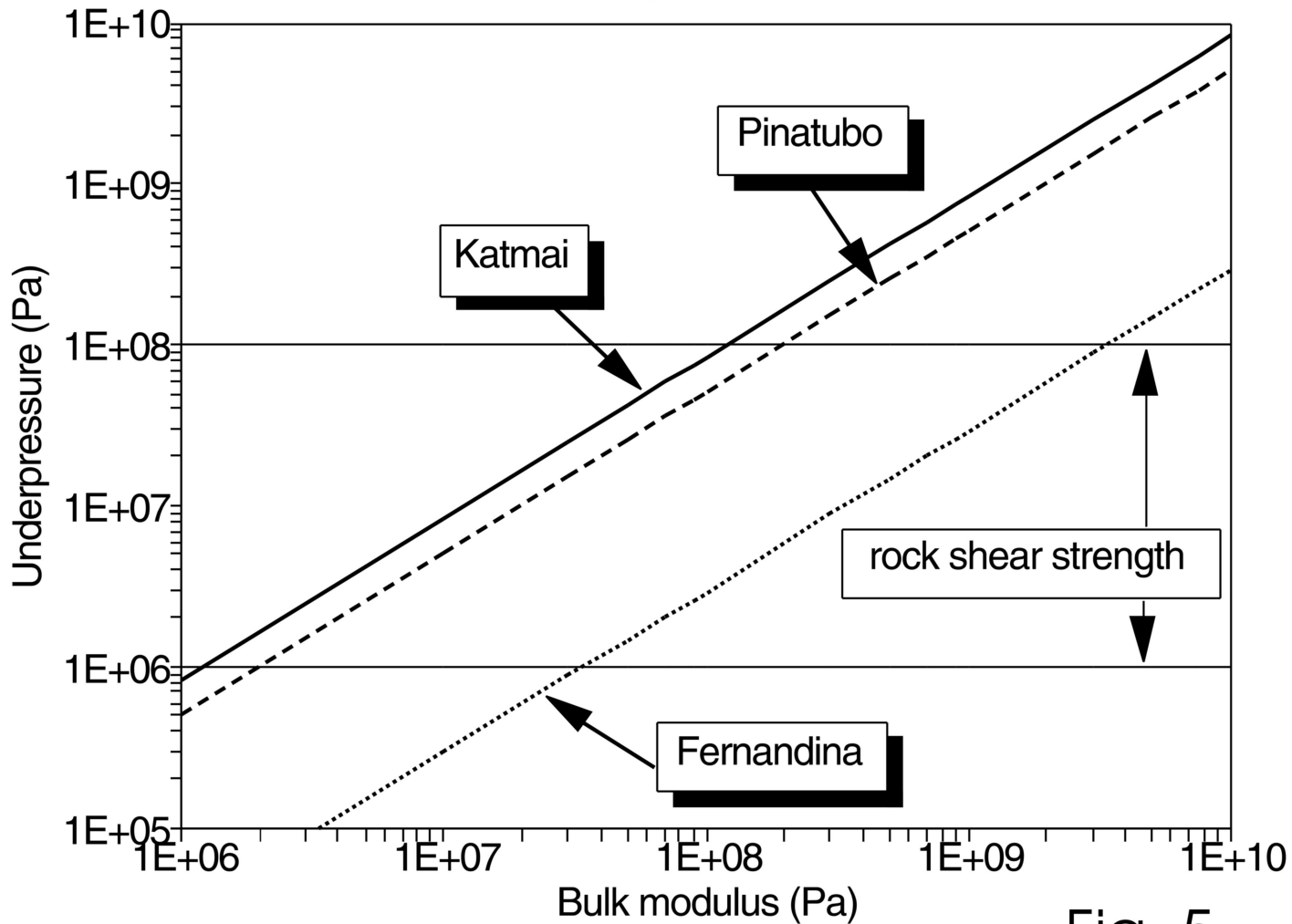
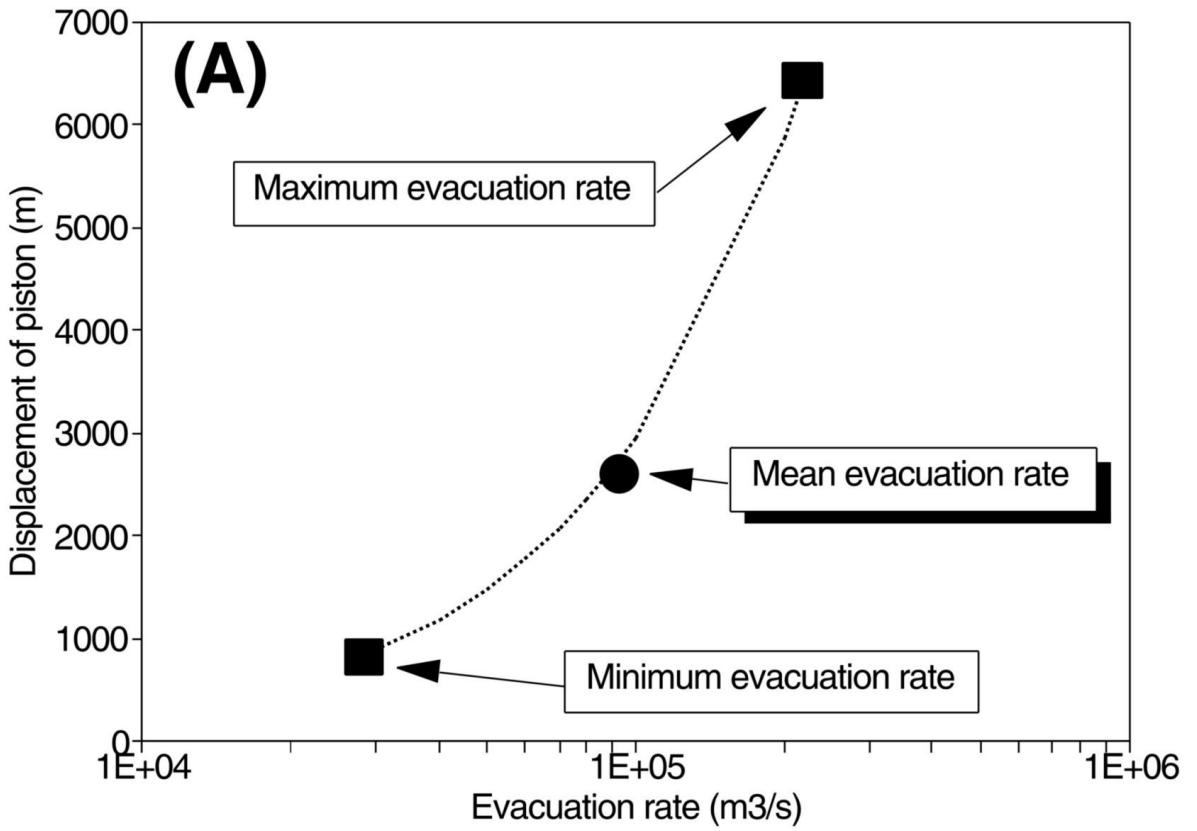


Fig. 5

# Katmai



# Pinatubo

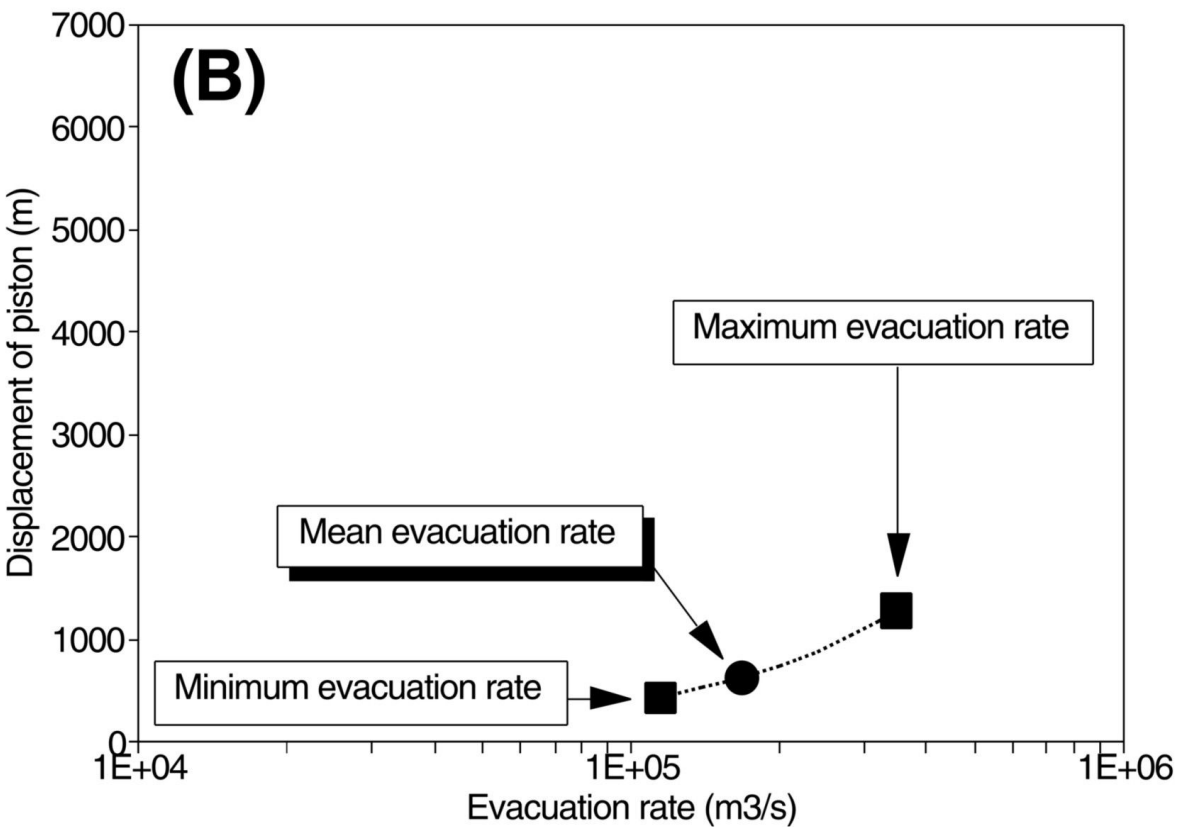
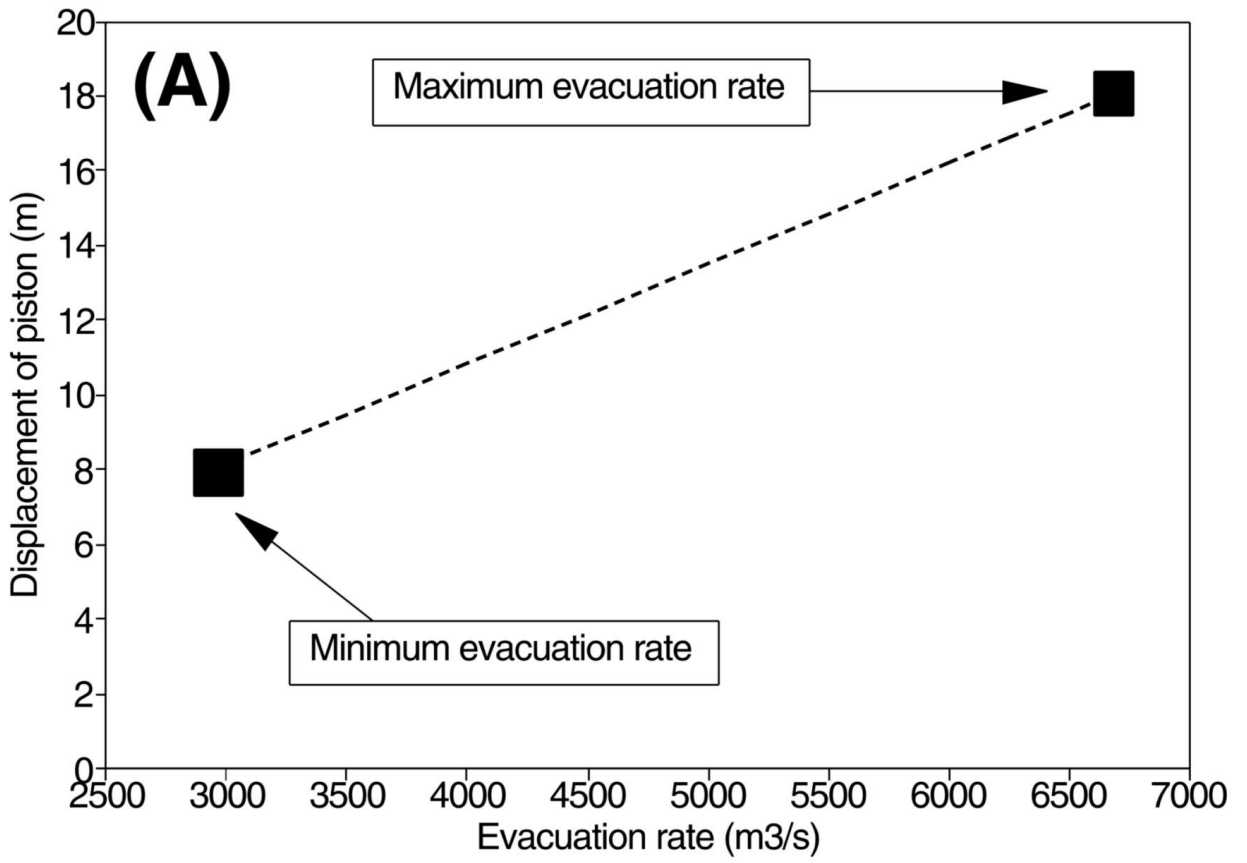


Fig. 6

### Evacuation rate



### Time interval

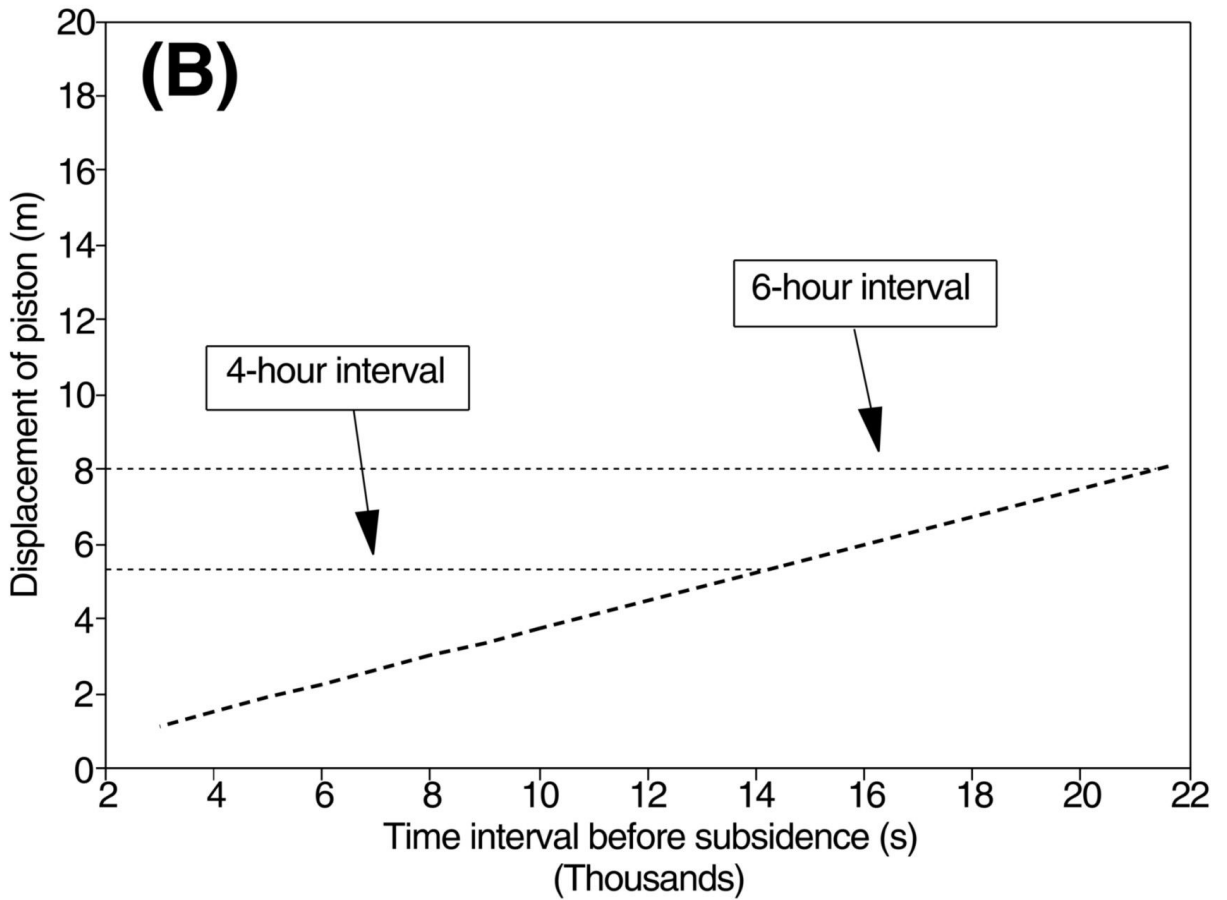


Fig. 7